Geological Magazine

www.cambridge.org/geo

Original Article

Cite this article: Qian F, Chang F, Nürnberg D, Zhang S, Wang Y, Zhang J, Tang L, and Li T. Precessional hydroclimatic synchronicity changes in the Indo-Pacific Warm Pool driven by the intertropical convergence zone over the past 450 kyr. *Geological Magazine* **161**(e9): 1–15. https://doi.org/10.1017/S0016756824000177

Received: 28 December 2023
Revised: 29 April 2024
Accepted: 1 June 2024

Keywords:
Indo-Pacific warm pool; tropical hydroclimate; intertropical convergence zone (ITCZ); precession

Corresponding authors:
Fengming Chang; Email: chfm@qdio.ac.cn;
Tiegang Li; Email: tgli@fio.org.cn

© The Author(s), 2024. Published by Cambridge University Press. This is an Open Access article, distributed under the terms of the Creative Commons Attribution-NonCommercial-NoDerivatives licence (http://creativecommons.org/licenses/by-nc-nd/4.0/), which permits non-commercial re-use, distribution, and reproduction in any medium, provided that no alterations are made and the original article is properly cited. The written permission of Cambridge University Press must be obtained prior to any commercial use and/or adaptation of the article.

Precessional hydroclimatic synchronicity changes in the Indo-Pacific Warm Pool driven by the intertropical convergence zone over the past 450 kyr

Fang Qian[1,2,3], Fengming Chang[1,4,5], Dirk Nürnberg[6], Shuai Zhang[7], Yi Wang[2], Junru Zhang[1,5], Luyao Tang[1,5] and Tiegang Li[4,8]

[1]Key Laboratory of Ocean Observation and Forecasting, Key Laboratory of Marine Geology and Environment, Institute of Oceanology, Chinese Academy of Sciences, Qingdao, China; [2]Department of Earth and Environmental Sciences, Tulane University, New Orleans, LA, USA; [3]Department of Geology and Geophysics, Woods Hole Oceanographic Institution, Woods Hole, MA, USA; [4]Laboratory for Marine Geology, Qingdao Marine Science and Technology Center, Qingdao, China; [5]University of Chinese Academy of Sciences, Beijing, China; [6]GEOMAR Helmholtz Center for Ocean Research Kiel, Kiel, Germany; [7]College of Oceanography, Hohai University, Nanjing, China and [8]Key Laboratory of Marine Geology and Metallogeny, First Institute of Oceanography, MNR, Qingdao, China

Abstract

The Indo-Pacific Warm Pool (IPWP) significantly influences the global hydrological cycle through its impact on atmospheric-oceanic circulation. However, gaining a comprehensive understanding of the hydrologic climate dynamics within the IPWP and its broader effects on the global climate have been hindered by spatial and temporal limitations in paleoclimate records on orbital timescales. In this study, we reconstructed precipitation records (approximated from $\delta^{18}O_{sw\text{-}ivc}$) over the past 450 kyr, based on planktonic foraminiferal Mg/Ca and $\delta^{18}O$ data obtained from International Ocean Discovery Program Site U1486 in the western tropical Pacific. The $\delta^{18}O_{sw\text{-}ivc}$ record revealed a generally consistent pattern with precession variations over the past 450 kyr, closely corresponding to changes in boreal summer insolation at the equator. The $\delta^{18}O_{sw\text{-}ivc}$ record displayed an anti-phased relationship with Chinese speleothem $\delta^{18}O$ records on the precession band, with lower precipitation in the western tropical Pacific and higher precipitation in the East Asia summer monsoon region during periods of high Northern Hemisphere summer insolation. This anti-phased correlation primarily resulted from the north-south migration of the Intertropical Convergence Zone (ITCZ), influenced by the interhemispheric insolation contrast. By considering additional $\delta^{18}O_{sw\text{-}ivc}$ records from various locations within the IPWP region, we identified synchronous precipitation changes within the IPWP on the precession band. The synchronization of precipitation on both margins of the ITCZ's seasonal range and differences between central and marginal regions of the ITCZ within the IPWP revealed the expansion and contraction of the ITCZ on precession band.

1. Introduction

The Indo-Pacific Warm Pool (IPWP), acknowledged as possessing the world's largest tropical warm water mass, is characterized by sea surface temperatures surpassing 28°C (Clement *et al.* 2005; Kim *et al.* 2012; De Deckker, 2016) and plays a crucial role in atmospheric deep convection (Russell *et al.* 2014). Variations in sea surface temperatures, rainfall patterns and oceanic circulation within the IPWP significantly impact the distribution of heat and moisture, thus influencing global atmospheric circulation patterns (Cane, 1998; Hoerling *et al.* 2001; Yan *et al.* 1992; Qian *et al.* 2023). Modern observations highlight the substantial impact of the seasonal latitudinal shifts of the Intertropical Convergence Zone (ITCZ) and its associated monsoon system, as well as the El Niño-Southern Oscillation (ENSO) variability, on shaping hydrologic characteristics in the IPWP region (Leech *et al.* 2013; Schneider *et al.* 2014). Therefore, studying hydrological climate variations in the IPWP is crucial for unraveling its intricate role in regional and global climate systems.

On geological timescales, the impact and mechanisms of ITCZ variations on the regional precipitation changes within the IPWP present conflicting findings. As a narrow band of convective winds and intense precipitation located near the equator, the ITCZ regulates the distribution of precipitation in the middle and low latitudes by seasonally migrating in response to interhemispheric temperature gradients (Schneider *et al.* 2014; Denniston *et al.* 2016). With the southward migration of the ITCZ, precipitation decreases in the Northern Hemisphere

https://doi.org/10.1017/S0016756824000177 Published online by Cambridge University Press

summer monsoon area, while increasing in the Southern Hemisphere summer monsoon area, and vice versa (Schneider *et al.* 2014). Several studies propose that tropical precipitation changes were primarily linked to the precession cycles in Earth's orbit (Clement *et al.* 2004; Wang *et al.* 2008; Merlis *et al.* 2013; Jalihal *et al.* 2019). Accordingly, the interhemispheric anti-phasing precipitation pattern is shaped by contrasting insolation between the Northern and Southern Hemispheres, causing latitudinal ITCZ migrations (Berger, 1978; Kutzbach *et al.* 2008). Findings from stalagmite $\delta^{18}O$ records in both hemispheres strongly support this hypothesis (e.g., Wang *et al.* 2008; Cheng *et al.* 2016). Reconstructions of precipitation, runoff and sea-surface salinity (SSS) from the IPWP further reveal notable responses to precession-induced alterations (e.g., Kissel *et al.* 2010; Tachikawa *et al.* 2011; Dang *et al.* 2015; Jian *et al.* 2022). Notably, Earth's obliquity also appears to be important in driving the latitudinal migration of the ITCZ, similarly resulting in anti-phase variations in interhemispheric precipitation in the IPWP (Liu *et al.* 2015; Zhang *et al.* 2020, 2022). Liu *et al.* (2015) suggest that obliquity forcing may have a greater impact on the western Pacific ITCZ migration, based on planktonic foraminifera REE/Ca records. Therefore, the reconstruction of precipitation records on longer timescales is of great significance for exploring the effects of diverse orbital forcing on the hydroclimate variability.

In contrast to the observed anti-phase precipitation patterns between hemispheres on different timescales, an increasing number of studies demonstrated synchronized precipitation variations between hemispheres in tropical regions on (sub-) millennial timescales (e.g., Konecky *et al.* 2013; Yan *et al.* 2015; Denniston *et al.* 2016; Scroxton *et al.* 2017; Yang *et al.* 2023). Such synchronized pattern would contradict the traditional migration theory of the ITCZ. The in-phase precipitation changes can be well explained by the expansion and contraction of the latitudinal extent of the ITCZ (Konecky *et al.* 2013; Yan *et al.* 2015; Denniston *et al.* 2016; Scroxton *et al.* 2017; Yang *et al.* 2023). During times of ITCZ expansion, precipitation intensifies synchronously at both northern and southern edges, while precipitation declines simultaneously at both edges when the ITCZ contracts (Yuan *et al.* 2023). The expansion and contraction of the ITCZ is likely triggered by various interacting factors, such as symmetrical changes in solar irradiance (Yan *et al.* 2015; Scroxton *et al.* 2017), strengthening Walker circulation (Konecky *et al.* 2013) and changes in the meridional atmospheric circulation (Denniston *et al.* 2016). Further studies, hence, are warranted to explore the impact of spatial ITCZ variations on alterations in precipitation patterns between hemispheres.

As the region with the highest water vapor exchange globally (Pierrehumbert, 2000), the IPWP is ideal to provide insight into the impact of ITCZ migration and expansion/contraction on local precipitation. Recently, Xiong *et al.* (2022) and Yu *et al.* (2023) examined the spatial pattern of precipitation variations across the IPWP on millennial scales, highlighting the importance of the ITCZ on the precipitation patterns in different regions of the IPWP. The observed changes in precipitation during the Last Glacial Maximum (LGM) point to an overall drying trend across the IPWP, caused by both the zonal shifts of ENSO and the meridional migration of ITCZ (Xiong *et al.* 2022). Yu *et al.* (2023) identified noticeably spatial heterogeneity of precipitation within the IPWP over the past 40 kyr, attributed to the predominant effects of the ENSO-like system in the western Pacific and the migration of the ITCZ in the Indian Ocean. Unfortunately, studies on past ITCZ expansion/contraction changes are not only scarce but also primarily confined to the last few millennia for the IPWP region (e.g., Denniston *et al.* 2016; Konecky *et al.* 2013; Scroxton *et al.* 2017; Yan *et al.* 2015; Yang *et al.* 2023), significantly limiting our understanding of the impact of ITCZ variability on spatial patterns of precipitation variations in IPWP.

To determine the temporal and spatial variability of the ITCZ on orbital timescales, we attempted to reconstruct the precipitation patterns within the IPWP region. Past precipitation, approximated from the residual oxygen isotope compositions of seawater, was deduced from combined $\delta^{18}O$ and Mg/Ca compositions of sea surface-dwelling planktonic foraminifera from International Ocean Discovery Program (IODP) Site U1486 within the central IPWP (Bismarck Sea). By integrating published ice-volume corrected sea surface salinity records ($\delta^{18}O_{sw\text{-}ivc}$) from the IPWP region, we assessed the spatial and temporal patterns of precipitation across the IPWP over the past 450 kyr and explored its driving mechanisms on the precession band.

2. Materials and methods

2.a. Location of site U1486 and modern climate

IODP Expedition 363 Site U1486 (02°22.34′S, 144°36.08′E) was drilled at a water depth of 1332 m in the Bismarck Sea, located ~150 km away from the mouth of the Sepik River in Papua New Guinea (Fig. 1a; Rosenthal *et al.* 2018). This study focused on samples from Site U1486, collected at 10-cm intervals, covering a depth range from the core-top down to 31 m Core Composite Depth Below Sea Floor. The sediment lithology in this section remained consistently homogenous, primarily composed of fine-grained, grayish-white sediment rich in planktonic microfossils. No volcanic ash layers or signs of disturbance were observed.

The hydrological cycle in the studied area is influenced both by the Asian-Australian monsoon and ENSO (Webster *et al.* 1998; Wang *et al.* 2003). During the boreal summer, southeasterly trade winds prevail, with the ITCZ shifting northward, thereby reducing the precipitation rate in the study area (Fig. 1a, c). Conversely, northwesterly winds dominate during the boreal winter, leading to a southward shift of the ITCZ and an increase in precipitation (Fig. 1a, c). On inter-annual timescales, precipitation is closely linked to ENSO events (Fig. 1b). Unusual dry (wet) conditions occur in the Papua New Guinea region during El Niño (La Niña) phases (Dai & Wigley, 2000).

2.b. Stable oxygen isotope and Mg/Ca analyses

Stable oxygen isotope ($\delta^{18}O$) and Mg/Ca analyses were conducted on the surface-dwelling planktonic foraminiferal species *Globigerinoides ruber* (white) extracted from 335 samples collected at 10-cm intervals downcore. Approximately 50 shells of *G. ruber* were selected from the 250–355 μm size fraction. Subsequently, these foraminiferal shells were gently crushed into several fragments.

For stratigraphical purposes, $\delta^{18}O$ was measured on the benthic foraminifer *Cibicidoides wuellerstorfi*. Approximately 3–5 individuals were picked from both the 300–355 μm and the 355–500 μm size fractions.

For stable isotope analysis, all fragments from the benthic samples and one-third of the fragments from the planktonic foraminifer *G. ruber* were utilized, while the remaining two-thirds of the *G. ruber* fragments were allocated for Mg/Ca analysis. The isotope analysis was performed using a GV IsoPrime mass spectrometer at the Key Laboratory of Marine Geology and

https://doi.org/10.1017/S0016756824000177 Published online by Cambridge University Press

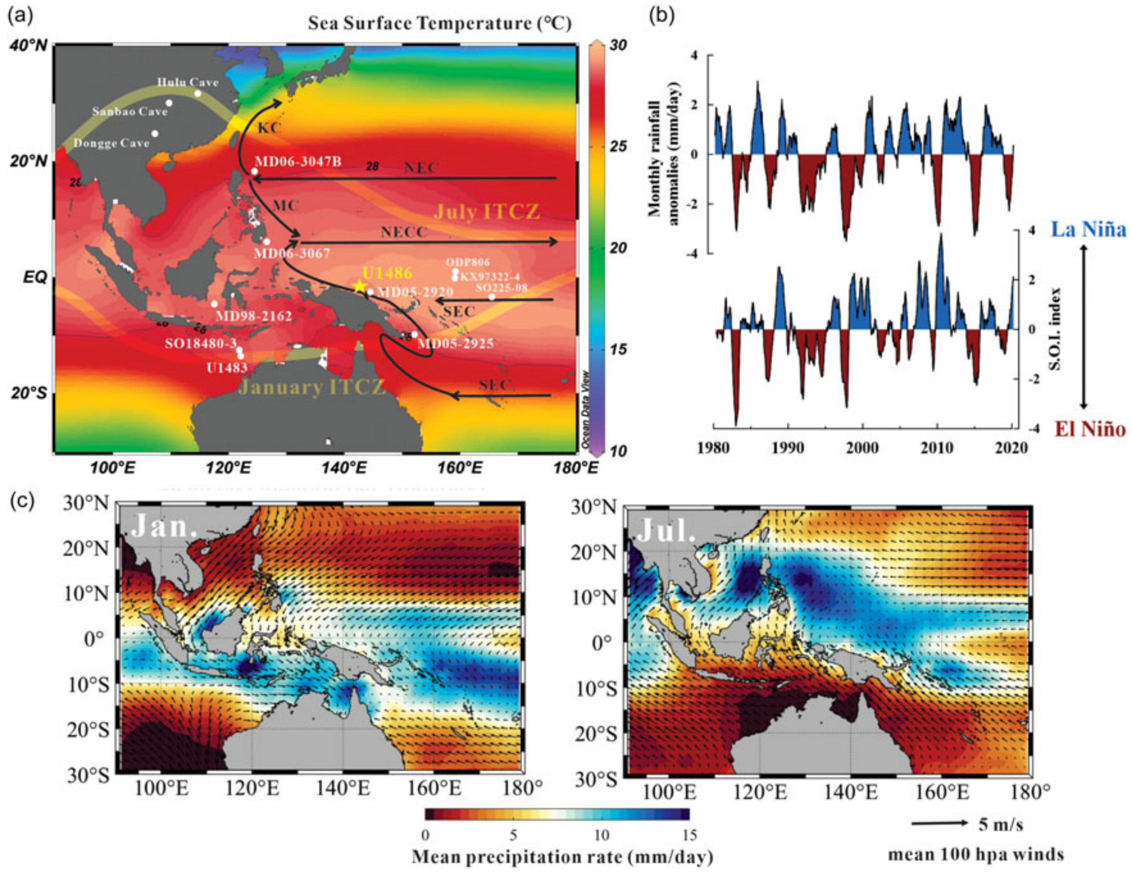

Figure 1. (Colour online) The Indo-Pacific Warm Pool and regional circulation patterns, alongside the modern climatology of the study area. (a) Map of the IPWP displaying modern annual sea surface temperatures (SST at 0 m; World Ocean Atlas 2013 dataset; Locarnini *et al.* 2013) of the studied Site U1486 (yellow star) and other relevant sites discussed in the study (white circles) is shown. Bright yellow shading lines denote the mean positions of the Intertropical Convergence Zone (ITCZ) in July and January, respectively (Lutgens & Tarbuck, 2001). Black dotted lines represent annual mean 28°C SST isotherms. Key ocean currents include the North Equatorial Current (NEC), North Equatorial Counter Current (NECC), South Equatorial Current (SEC), Kuroshio Current (KC) and Mindanao Current (MC). (b) The Southern Oscillation Index (SOI, 5-point running average) between 1980 and 2020 (https://www.cpc.ncep.noaa.gov/data/indices/soi) together with the monthly rainfall anomaly over the Site U1486 source area (2.5° spatial resolution centered on 2°S, 144°E, 11-point running average, https://climatedataguide.ucar.edu/climate-data/gpcp-monthly-global-precipitation-climatology-project). (c) Depiction of mean rainfall rate and the 1000 hPa wind field in January (left) and July (right). Rainfall data sourced from https://psl.noaa.gov/data/gridded/data.cmap.html, while land wind data obtained from http://iridl.ldeo.columbia.edu/expert/ds:/SOURCES/.NOAA/.NCEP-NCAR/.CDAS-1.

Environment, Institute of Oceanography, Chinese Academy of Sciences, Qingdao. Results are presented in $\delta^{18}O$ notation (‰ relative to the Vienna Pee Dee Belemnite standard), calibrated to the National Bureau of Standards 18 standard, analyzed approximately every 10 samples, with a long-term standard deviation of 0.06‰.

For Mg/Ca analysis, the *G. ruber* underwent pretreatment and cleaning procedures following the methods described by Barker *et al.* (2003), with the exclusion of a reductive step. The shells were sequentially cleaned using Milli-Q water rinses, methanol rinses and an oxidizing solution. Organic matter was eliminated through oxidation using a heated 1% NaOH-buffered H_2O_2 solution. Samples were dissolved in 0.075-M QD HNO_3 and analyzed using an inductively coupled plasma–optical emission spectrometer (ICP-OES) at the same laboratory. The average standard deviation for replicate measurements was approximately 0.52%. The contamination assessment included Fe/Ca, Mn/Ca and Al/Ca ratios, with most samples registering values below detection limits (Fig. S1). Furthermore, according to Barker *et al.* (2003), the presence of detrital contamination affecting the measured Mg/Ca ratios can be inferred by evaluating the correlation between estimated Mg/Ca and Fe/Ca or Al/Ca data. No significant correlation was found between Fe/Ca and Mg/Ca ($R^2 = 0.006$), Mn/Ca and Mg/Ca ($R^2 = 0.02$), or Al/Ca and Mg/Ca ($R^2 = 0.004$), ensuring the reliability of the Mg/Ca measurements (Fig. S1).

2.c. Estimates of sea-surface temperature and seawater $\delta^{18}O$

The planktonic foraminifer *G. ruber* calcifies within the depths of 30–95 m in the mixed layer of the Western Pacific Warm Pool (WPWP) (Rippert *et al.* 2016; Raddatz *et al.* 2017). By comparing the reconstructed sea-surface temperature ($SST_{Mg/Ca}$) based on the Mg/Ca ratio in *G. ruber* shells using available calibration equations (Fig. S2; Table S1), we selected the equation (1) established in the western Pacific by Dekens *et al.* (2002). This decision was based on the fact that its constructed average core-top $SST_{Mg/Ca}$ value (~29.3°C) aligns closely with the modern SST (~29.1°C; Locarnini *et al.* 2013).

$$\begin{aligned} \text{SST}\ (^\circ\text{C}) \ &= \ \ln\left[\text{Mg/Ca}\ (\text{mmol/mol})/0.38\right]/0.09 \\ &\quad + 0.61\ (\text{core depth km}) + 1.6 \end{aligned} \tag{1}$$

Calcite dissolution might lead to lowered Mg/Ca-temperature estimates due to the selective removal of Mg-ions from the foraminiferal calcite (e.g., Nürnberg *et al.* 1996; Dekens *et al.* 2002;

Regenberg *et al.* 2006). Equation (1) incorporates a depth correction to account for dissolution effects on Mg/Ca. As indicated by Regenberg *et al.* (2014), foraminiferal Mg/Ca in the study area is notably affected at depths below 2500 m. Given the limited impact of dissolution at our specific location (1332 m), we decided not to apply the dissolution correction in our Mg/Ca data. Moreover, recent calibrations derived from sediment traps and modern core tops in WPWP provide confidence that the dissolution effect is insignificant in our study area (Hollstein *et al.* 2017).

The error in $SST_{Mg/Ca}$ reconstructions was assessed by propagating the uncertainties arising from both the Mg/Ca measurements and the Mg/Ca temperature calibration, following Mohtadi *et al.* (2014). On average, the resulting errors are approximately ±0.97°C.

The oxygen isotope composition of seawater ($\delta^{18}O_{sw}$) and SSS exhibit a linear relationship in the western Pacific (e.g., Fairbanks *et al.* 1997; Gibbons *et al.* 2014). As a result, the residual $\delta^{18}O$ of surface seawater ($\delta^{18}O_{sw\text{-}ivc}$), which corrects for the influence of continental ice volume, has been widely utilized in the reconstruction of past regional hydrological changes. We derived $\delta^{18}O_{sw}$ using Equation (2) established by Bemis *et al.* (1998), adjusting values to the Vienna Standard Mean Ocean Water standard by adding 0.27‰ (Hut, 1987). The estimated average core-top $\delta^{18}O_{sw}$ value (~0.25‰) closely matches the modern seawater $\delta^{18}O$ value at the core site (0.22‰; LeGrande & Schmidt, 2006). Additionally, we compared the estimated $\delta^{18}O_{sw}$ results derived from different $SST_{Mg/Ca}$ calibration equations (Fig. S2; Table S1), validating the reliability of the calibration equations. Furthermore, we corrected $\delta^{18}O_{sw}$ for global ice volume changes based on the studies by Bintanja *et al.* (2005) and Spratt & Lisiecki (2016), respectively. As shown in Fig. S2, the two estimated $\delta^{18}O_{sw\text{-}ivc}$ results exhibit a high level of consistency. Consequently, the estimated $\delta^{18}O_{sw\text{-}ivc}$ derived from simulated global marine isotopes from Bintanja *et al.* (2005) is reliable and feasible.

$$\delta^{18}O_{sw} = \left[SST_{Mg/Ca}(^{\circ}C) - 16.5 + 4.8 \times \delta^{18}O_{G.\ ruber}\right]/4.8 + 0.27 \quad (2)$$

We calculated uncertainties in $\delta^{18}O_{sw\text{-}ivc}$ using the method described by Mohtadi *et al.* (2014), accounting for uncertainties from Mg/Ca and $\delta^{18}O$ measurements, temperature equations and global ice volume removal (Bintanja *et al.* 2005). The resulting uncertainties averaged 0.21‰ for $\delta^{18}O_{sw\text{-}ivc}$.

2.d. Chronology

The age model for Site U1486 was constructed based on the $\delta^{18}O$ record obtained from the benthic foraminifer *Cibicidoides wuellerstorfi* ($\delta^{18}O_{C.\ wuellerstorfi}$). The $\delta^{18}O_{C.\ wuellerstorfi}$ values ranged from 1.68‰ to 3.85‰ over the past 450 kyr BP, revealing clear glacial-interglacial cycles (Fig. 2a). Comparison of $\delta^{18}O_{C.\ wuellerstorfi}$ values with the global benthic foraminiferal $\delta^{18}O$ stack LR04 (Lisiecki & Raymo, 2005) identified 15 tie points for age control (Fig. 2a). The age model for the entire core was calculated using a MATLAB linear interpolation optimization method. Site U1486 provides a continuous record spanning the past 450 kyr, encompassing five glacial-interglacial cycles (Fig. 2a). The average sedimentation rate over this period was approximately 7.17 cm/kyr the past 450 kyr (Fig. 2b). With a sampling interval of 10 cm, the average sample resolution is approximately 1.3 kyr.

3. Results

The oxygen isotope values of *G. ruber* ($\delta^{18}O_{G.\ ruber}$) exhibit a range from −3.18‰ to −0.93‰ over the past 450 kyr, displaying distinct glacial-interglacial cycles (Fig. 3a). Generally, $\delta^{18}O_{G.\ ruber}$ values are higher/heavier during glacial periods (MIS 2, 4, 6, 8, 10 and 12) and lower/lighter during interglacial stages. The highest $\delta^{18}O_{G.\ ruber}$ value (−0.93‰) is observed at ~433.4 kyr (MIS 12), while the lowest $\delta^{18}O_{G.\ ruber}$ value (~−3.18‰) is found at the top of the core.

G. ruber Mg/Ca varies from 3.22 to 5.24 mmol/mol, which yields sea-surface temperature ($SST_{Mg/Ca}$) at Site U1486 spanning a range of 25.3 to 30.8 °C, with an average of approximately 27.7 °C. As shown in Figure 3b, the $SST_{Mg/Ca}$ record shows pronounced glacial-interglacial variations over the past 450 kyr, with higher temperatures occurring during interglacial stages and lower temperatures during peak glacial stages.

Modern seawater $\delta^{18}O$ and SSS display a positive correlation, with higher $\delta^{18}O_{sw\text{-}ivc}$ values corresponding to increased salinity in surface seawater, while lower $\delta^{18}O_{sw\text{-}ivc}$ values indicate fresher seawater (Fairbanks *et al.* 1997; Rosenthal *et al.* 2003; Stott *et al.* 2004; Gibbons *et al.* 2014). Model simulations also support the assumption that the tropical Pacific has maintained a consistent relationship between $\delta^{18}O_{sw\text{-}ivc}$ and SSS (Holloway *et al.* 2016). In comparison with $\delta^{18}O_{G.\ ruber}$ and $SST_{Mg/Ca}$, $\delta^{18}O_{sw\text{-}ivc}$ does not exhibit obvious glacial-interglacial cycles, ranging from −0.66‰ to 1.20‰ (Fig. 3c). However, during MIS 2, MIS 6, MIS 10 and MIS 12, $\delta^{18}O_{sw\text{-}ivc}$ is relatively lower compared to the interglacial stages, with the highest value observed near the MIS 10/9 transition (Fig. 3c). During deglacial episodes of rapid $SST_{Mg/Ca}$ warming (e.g., MIS 12/11, MIS 10/9, MIS 6/5 and MIS 2/1), sea-surface $\delta^{18}O_{sw\text{-}ivc}$ values simultaneously increase, implying a change to more saline conditions at sea surface (Fig. 3b, c).

4. Discussion

4.a. Using site U1486 $\delta^{18}O_{sw\text{-}ivc}$ as a proxy to reconstruct local precipitation variability over the past 450 kyr

$\delta^{18}O_{sw}$ serves as a common proxy for SSS, which is a crucial parameter in the hydrological cycle (Stott *et al.* 2004; Leech *et al.* 2013). Although $\delta^{18}O_{sw}$ is influenced by multiple factors, including precipitation, evaporation, upwelling and meridional and zonal currents (Conroy *et al.* 2017), the existence of a linear correlation between $\delta^{18}O_{sw}$ and SSS is due to both being primarily influenced by evaporation and precipitation (Fairbanks *et al.* 1997; LeGrande & Schmidt, 2006). Thus, the $\delta^{18}O_{sw}$ variability is often interpreted in the context of hydroclimate variability (Fairbanks *et al.* 1997; LeGrande & Schmidt, 2006). Additionally, Conroy *et al.* (2017) found that the $\delta^{18}O_{sw}$-salinity linear relationship appears stronger in the western tropical Pacific based on both observational data and results from isotope-enabled climate model simulations. Therefore, $\delta^{18}O_{sw}$ primarily reflects changes in the precipitation-evaporation balance. Given the minimal fluctuations in modern SST in the western Pacific (Kim *et al.* 2012), $\delta^{18}O_{sw}$ likely reflects local precipitation patterns (Gibbons *et al.* 2014). Recent studies by Yang *et al.* (2024) analyzing modern reanalysis data in the South China Sea revealed an inverse correlation between regional SSS and precipitation rate. Additionally, Conroy *et al.* (2017) identified a weak relationship between SST and SSS in the western Pacific based on modern data.

For the reconstruction of past local precipitation changes in the western Pacific, we consider the ice-volume corrected $\delta^{18}O_{sw\text{-}ivc}$ record from Site U1486. Positive deviations in $\delta^{18}O_{sw\text{-}ivc}$ values

https://doi.org/10.1017/S0016756824000177 Published online by Cambridge University Press

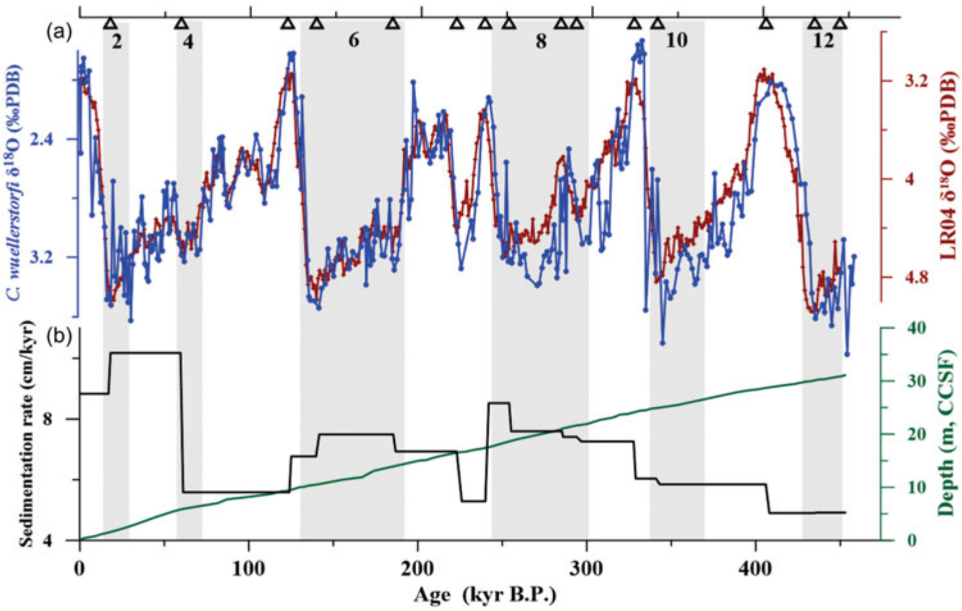

Figure 2. (Colour online) Age model of Site U1486. (a) Benthic foraminifer *C. wuellerstorfi* $\delta^{18}O$ (blue line) and the global benthic foraminiferal $\delta^{18}O$ stack LR04 (Lisiecki & Raymo, 2005) (red line). Black triangles indicate tie points for $\delta^{18}O_{C.\ wuellerstorfi}$. (b) Depth-age model (green line) and sedimentation rates (black line) of sediment Site U1486. Gray vertical shadings indicate even-numbered Marine Isotope Stages (MIS).

indicating more saline conditions at sea surface, suggest reduced local precipitation in the western Pacific, while negative values point to intensified local precipitation (Rosenthal *et al.* 2003; Stott *et al.* 2004). The Site U1486 $\delta^{18}O_{sw\text{-}ivc}$ record displays relatively muted glacial-interglacial cycles over the past 450 kyr, which fluctuate between −0.66 ‰ and 1.20 ‰ and differ substantially from the $SST_{Mg/Ca}$ pattern (Fig. 3c). Moreover, the variation in Site U1486 $\delta^{18}O_{sw\text{-}ivc}$ is similar to the change in the ln(Ti/Ca) record obtained from the adjacent core MD05-2920 (Fig. 4i; Tachikawa *et al.* 2011, 2014). The ln(Ti/Ca) values were utilized as an indicator of rainfall over the drainage basin of the Sepik River in New Guinea (Tachikawa *et al.* 2011, 2014). Cross-spectral analysis reveals a significant coherence between Site U1486 $\delta^{18}O_{sw\text{-}ivc}$ and ln(Ti/Ca) from core MD05-2920 on the precession band (Fig. S3), supporting the dominance of precession cycles in controlling precipitation variations in the study area.

To study the underlying mechanisms driving local precipitation changes in the western Pacific over the past 450 kyr, we employed redfit spectral and wavelet analysis using the Past3 software with a Hanning window (Hammer *et al.* 2001). The spectral analysis reveals that the Site U1486 $\delta^{18}O_{sw\text{-}ivc}$ record is characterized by prominent 100 kyr eccentricity and 23 kyr precession cycles. Wavelet analyses further shows that the 23 kyr cycle is most prominent during ~260−180 and ~370−300 ka BP (Fig. 3e). The phase difference between the maximum in $\delta^{18}O_{sw\text{-}ivc}$ and the maximum in precession is ~−148° (Fig. 5h). On the precession band, the Site U1486 $\delta^{18}O_{sw\text{-}ivc}$ record displays precession band-pass filtered patterns that are mostly in phase with a few exceptions, such as $\delta^{18}O_{sw\text{-}ivc}$ changes preceding precession shifts during the periods of ~175−145 and ~110−75 ka BP (Fig. 4j). The discrepancies between the $\delta^{18}O_{sw\text{-}ivc}$ and precession may be attributed to terrestrial influences (Hollstein *et al.* 2020), or due to a relatively weakened 23 kyr cycle during these specific time intervals (Fig. 3e). Nonetheless, the $\delta^{18}O_{sw\text{-}ivc}$ record exhibits an overall consistency with precession variations over the past 450 kyr, where almost every low precession value corresponds to high $\delta^{18}O_{sw\text{-}ivc}$ values (Fig. 4j). We conclude that the past local precipitation variations at Site U1486 were associated with precessional changes.

It is noteworthy that, although Site U1486 $\delta^{18}O_{sw\text{-}ivc}$ record and the ln(Ti/Ca) record from adjacent core MD05-2920 exhibit nearly coherent variation on the precession band (Fig. 4i, j), the ln(Ti/Ca) record is characterized by not only precession but also obliquity signals (Tachikawa *et al.* 2014). The coarse terrigenous fraction represented by Ti varied with the precession cycle, while $CaCO_3$ exhibited a pronounced obliquity band (Tachikawa *et al.* 2011). Additionally, precipitation records based on ln(K/Ca) at Site U1483 (offshore north-western Australia) contain an additional obliquity component (Zhang *et al.* 2020). The orbital forcing of elemental ratios is evidently different from the predominant precession control observed in the $\delta^{18}O_{sw\text{-}ivc}$ records of Site U1486. This discrepancy in dominant cyclicity may suggest that different precipitation proxies respond differently to climatic forcing. The SSS proxy ($\delta^{18}O_{sw\text{-}ivc}$), primarily controlled by the precipitation-evaporation balance (Conroy *et al.* 2017), tends to exhibit stronger precession-driven variability due to its direct linkage with monsoon dynamics and seasonal changes in precipitation (Stott *et al.* 2004).

Orbital precession is triggered by the Earth's rotational axis oscillation, leading to a continuous change in the relative positioning of the Earth and the Sun (Berger & Loutre, 1994). This alteration modifies the seasonal and meridional distribution of solar radiation across the Earth's surface with a 23 kyr periodicity (Berger & Loutre, 1994; Merlis *et al.* 2013). The equatorial insolation variation is primarily influenced by precession changes on orbital timescales, with an increased summer solar insolation in the equatorial region during low precession periods (Yin *et al.* 2021). Our $\delta^{18}O_{sw\text{-}ivc}$ record reveals a similar pattern with July–August insolation changes at the equator over the past 450 kyr. The elevated insolation levels corresponded to increased $\delta^{18}O_{sw\text{-}ivc}$ values, implying reduced local precipitation in Papua New Guinea, and vice versa (Fig. 4j). The core MD05-2920 ln(Ti/Ca) also exhibits significant coherence with insolation at precessional periodicities, consistent with our $\delta^{18}O_{sw\text{-}ivc}$ record of Site U1486 (Fig. 4i, j). Additionally, modeled precipitation results

https://doi.org/10.1017/S0016756824000177 Published online by Cambridge University Press

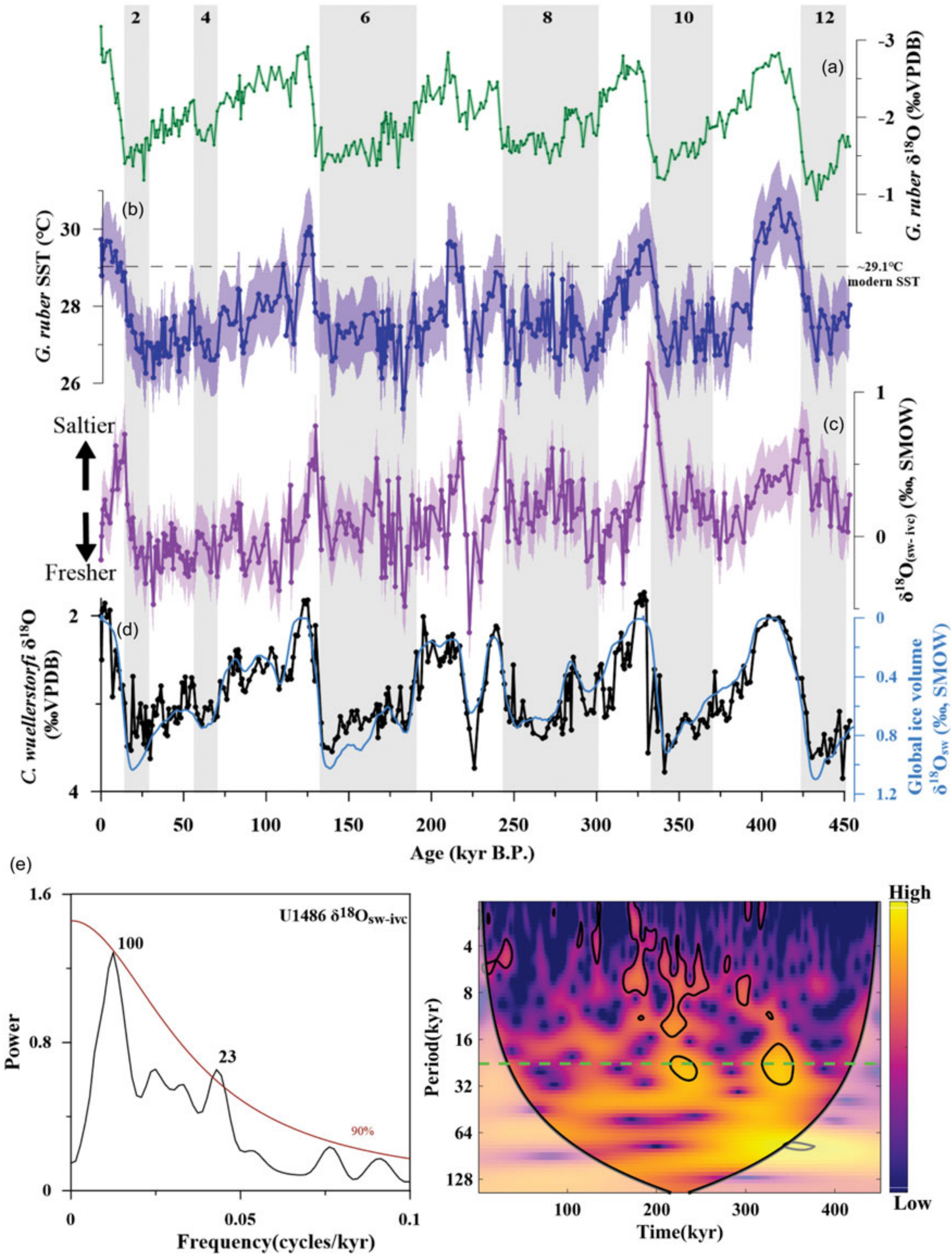

Figure 3. (Colour online) Planktonic foraminiferal proxy records of Site U1486. (a) *G. ruber* $\delta^{18}O$, (b) *G. ruber* Mg/Ca-based SST, (c) the ice volume corrected-seawater $\delta^{18}O$ ($\delta^{18}O_{sw\text{-}ivc}$) and (d) *C. wuellerstorfi* $\delta^{18}O$ (black), superimposed is the global ice volume $\delta^{18}O_{sw}$ (blue; Bintanja *et al*. 2005). Gray vertical shadings indicate even-numbered marine isotope stages (MIS), while colored shadings for individual records represent their respective error ranges (see Sections 2.2 and 2.3). (e) Spectral (left) and wavelet transform (right) analyses of the $\delta^{18}O_{sw\text{-}ivc}$ record of Site U1486. The green line indicates the precession cycle.

further support the simultaneous changes in precipitation and local summer insolation in the western Pacific (Kutzbach *et al*. 2008). These findings suggest that variations in local precipitation in the Papua New Guinea region were likely driven by the equatorial insolation changes in line with precessional variations. The precession signal might have influenced the local precipitation patterns through northern and southern hemispheric thermal gradients (Braconnot *et al*. 2008) or the temperature contrast between land and sea surfaces (Ruddiman, 2008; Merlis *et al*. 2013).

https://doi.org/10.1017/S0016756824000177 Published online by Cambridge University Press

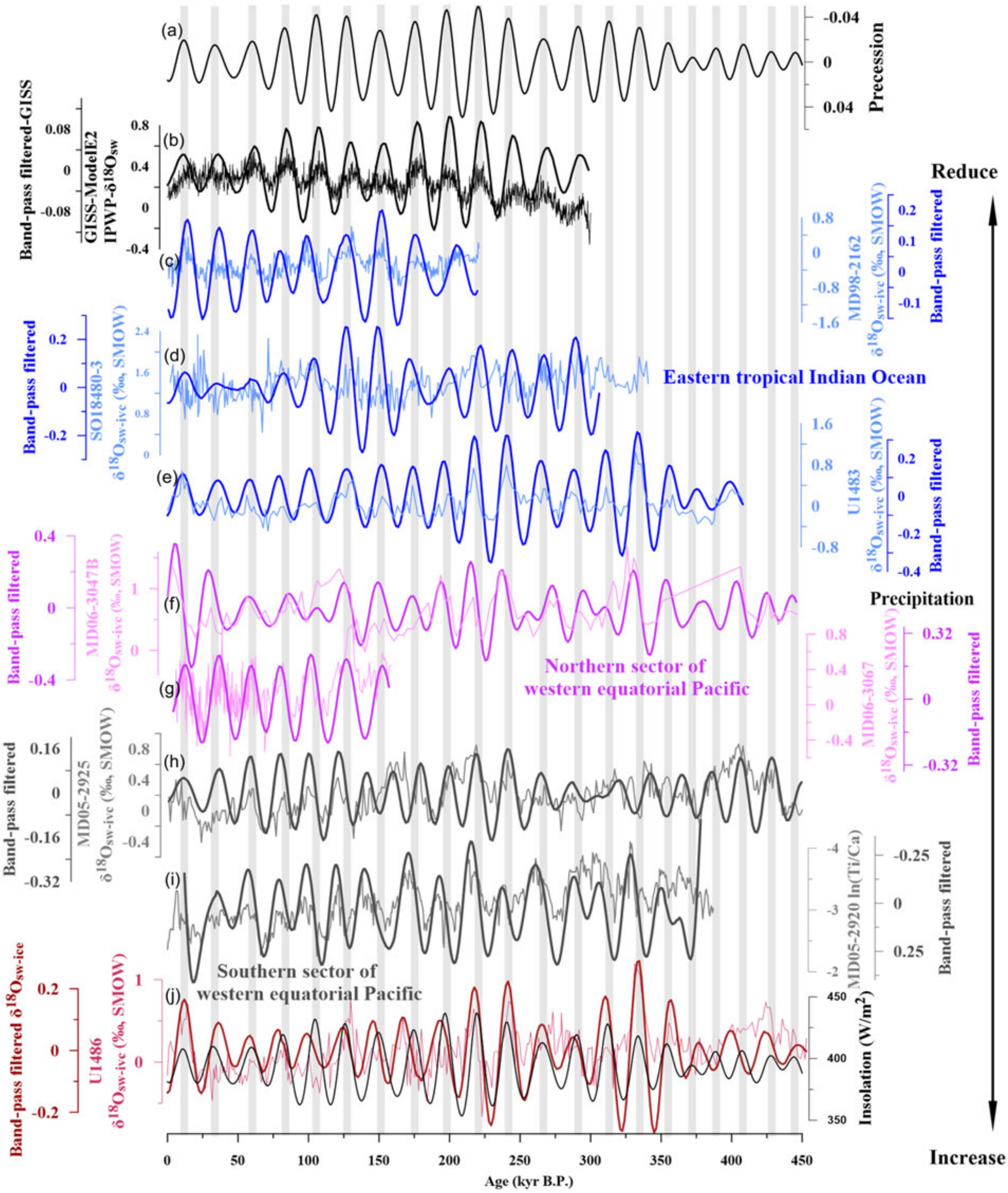

Figure 4. (Colour online) The orbital-scale precipitation pattern in the Indo-Pacific Warm Pool over the past 450 kyr. (a) The variation in precession (Laskar *et al.* 2004). (b) GISS_ModelE2-R simulated $\delta^{18}O_{sw\text{-}ivc}$ records of the IPWP (Jian *et al.* 2022). (c, d, e) The $\delta^{18}O_{sw\text{-}ivc}$ records of cores MD98-2162, SO18480-3 and U1483 in the eastern tropical Indian Ocean (Jian *et al.* 2022; Zhang *et al.* 2022). (f, g) The $\delta^{18}O_{sw\text{-}ivc}$ records of cores MD06-3047B and MD06-3067 in the northern sector of western equatorial Pacific (Bolliet *et al.* Bolliet *et al.*, 2011; Jia *et al.* Jia *et al.*, 2018). (h) The $\delta^{18}O_{sw\text{-}ivc}$ records of core MD05-2925 (Lo *et al.* 2022). (i) The ln(Ti/Ca) record of core MD05-2920 (Tachikawa *et al.* 2014). (j) The $\delta^{18}O_{sw\text{-}ivc}$ record of Site U1486, superimposed by the July–August insolation at the equator (black) (Laskar *et al.* 2004). The overlain, bold, dark-colored lines represent the precession band-pass filtered results. Band-pass filter with a central frequency of 0.043 kyr^{-1} and a bandwidth of 0.01 kyr^{-1}. Vertical grey bars indicate lower precession values.

4.b. Precession-driven synchronous precipitation changes in the IPWP over the past 450 kyr

The IPWP as Earth's largest reservoir of atmospheric water vapor experiences the highest rainfall levels (Cane, 1998; Leung *et al.* 2022). Modern mean rainfall data show a central region for rainfall within the IPWP (Fig. 1c). To investigate precipitation variations on orbital timescales across the entire IPWP region, we compared precipitation records from different areas within its central precipitation zone (Fig. 1a). These areas encompass the northern IPWP (cores MD06-3047B and MD06-3067; Bolliet *et al.* Bolliet *et al.*, 2011; Jia *et al.* Jia *et al.*, 2018), the southern sector of the IPWP (cores U1486 and MD05-2925; this study and Lo *et al.* 2022) and the Indian Ocean (cores MD98-2162, SO18480-3 and U1483; Jian *et al.* 2022; Zhang *et al.* 2022). We distinguish the northern and southern divisions of the IPWP based on the equator. Detailed information about the original datasets for these cores is provided in Table S2. Conroy *et al.* (2017) identified a linear relationship between $\delta^{18}O_{sw}$ and SSS in various IPWP areas across multiple sites. $\delta^{18}O_{sw\text{-}ivc}$ likely serves as a reliable proxy to reflect past local precipitation variations due to the limited variability of SST in the IPWP (Gibbons *et al.* 2014). All $\delta^{18}O_{sw\text{-}ivc}$ records are similarly based on *G. ruber* Mg/Ca and $\delta^{18}O$ and are considered to reliably reflect local precipitation through time.

All $\delta^{18}O_{sw\text{-}ivc}$ records from various regions of the western tropical Pacific across the equator suggest overall synchronous precipitation patterns on orbital timescales. The $\delta^{18}O_{sw\text{-}ivc}$ record of core MD05-2925 (Lo *et al.* 2022), situated in the southern region of the western equatorial Pacific, shows a fundamental synchrony with variations in boreal summer insolation at the equator driven by precession over the past 450 kyr (Fig. 4h). Similarly, the precipitation record of core MD06-3047B (Jia *et al.* Jia *et al.*, 2018), located in the northernmost part of the WPWP, is consistently related to precession variations over the past 450 kyr, except during the ~410-370 ka BP period (Fig. 4f) (likely due to missing original data in the core MD06-3047B $\delta^{18}O_{sw\text{-}ivc}$ record during this specific period). Furthermore, the filtered 23-kyr component of the $\delta^{18}O_{sw\text{-}ivc}$ record from core MD06-3067 in the northern IPWP also demonstrates synchronous changes with precession variations over the past ~160 kyr, where each peak in SSS corresponds to both a low in precession and a peak in equatorial insolation during boreal summer (Fig. 4g; Bolliet *et al.* Bolliet *et al.*, 2011).

In contrast, the $\delta^{18}O_{sw\text{-}ivc}$ record from the central IPWP core KX97322-4 exhibits limited coherence with precession variability over the past 360 kyr (Zhang *et al.* 2021). This lack of coherence might be attributed to an ENSO-like state or potentially to the fact that $\delta^{18}O_{sw\text{-}ivc}$ is influenced by both precession and obliquity (Zhang *et al.* 2015, 2021). Obliquity may affect the atmospheric circulation and the associated meridional heat and moisture fluxes by regulating the latitudinal distribution of insolation (Mantsis *et al.* 2011, 2014; Bosmans *et al.* 2015). This might explain why obliquity bands are present in the $\delta^{18}O_{sw\text{-}ivc}$ record of core KX97322-4, as obliquity could affect local precipitation through atmospheric circulation and heat and moisture fluxes. Additionally, variations in the $\delta^{18}O_{sw\text{-}ivc}$ signals may be due in part to differences in core locations capturing divergent information. Moreover, Liu *et al.* (2015) proposed that precipitation variations in the western Pacific are more affected by obliquity than by precession-paced changes in the ITCZ, based on foraminiferal rare earth elements (indicator of precipitation-dependent river runoff). This change in dominant cyclicity could be attributed to differences in proxy-specific bias or tendency. In the eastern IPWP, the $\delta^{18}O_{sw\text{-}ivc}$ records from cores SO225-08 (unpublished data from Nürnberg) and ODP806 (Lea *et al.* 2000), located in the eastern IPWP, did not exhibit synchronous changes with precession parameters but rather showed distinct glacial-interglacial cycles. This discrepancy might be attributed to the relatively low sample resolution in these records. Cores SO225-08 and ODP806, being situated close to the central equatorial Pacific, might experience more influence on their hydrological conditions by atmospheric circulation, such as the meridional Hadley circulation and the Walker circulation (Lea *et al.* 2000). In conclusion, the variations in $\delta^{18}O_{sw\text{-}ivc}$ across various regions of the WPWP are not entirely identical, possibly due to regional differences, varying impact of driving factors, and/or sample resolution. However, with respect to precessional cyclicity, all precipitation records within the central precipitation zone across the WPWP generally show similar patterns (Fig. 4).

Notably, the pattern of precipitation changes in the western part of the IPWP (eastern tropical Indian Ocean) is similar to in the western tropical Pacific. The filtered 23-kyr component of the $\delta^{18}O_{sw\text{-}ivc}$ records from the southern part of the Makassar Strait (core MD98-2162) and Timor Sea (cores SO18480-3 and U1483) close to the equator demonstrate a nearly synchronous response to precession-driven boreal summer insolation variations (Fig. 4c–e; Jian *et al.* 2022; Zhang *et al.* 2022). Higher insolation levels correspond to higher $\delta^{18}O_{sw\text{-}ivc}$ values, hence more saline sea-surface conditions, while lower insolation levels correspond to lowered $\delta^{18}O_{sw\text{-}ivc}$ values and fresher conditions (Fig. 4c–e). This covariance is consistent with the precipitation record of Site U1486. Overall, nearly all records are characterized by higher $\delta^{18}O_{sw\text{-}ivc}$ values (higher SSS; lower precipitation) at precession minima, implying that both the eastern tropical Indian Ocean and the western tropical Pacific within the IPWP experienced drier conditions simultaneously during lower precession periods (Fig. 4).

Consistently, the simulated annual mean $\delta^{18}O_{sw\text{-}ivc}$ derived from a water isotope ($\delta^{18}O_{sw}$)-enabled air-sea coupled climate model (GISS_ModelE2-R; Jian *et al.* 2022) reveals a dominant 23-kyr cycle with higher $\delta^{18}O_{sw\text{-}ivc}$ values and hence, more saline conditions at sea surface during precession minima (Fig. 4b), supporting our notion on synchronous precession-driven precipitation changes in the IPWP. We conclude that the variations in equatorial insolation, driven by precession parameters, likely influence the SSS through precipitation variability within the IPWP region.

4.c. Effects of the ITCZ changes on the precipitation variations in IPWP

4.c.1. Variations in ITCZ latitudinal migration

The IPWP is a significant moisture source for the East Asian summer monsoon (EASM). Numerous studies demonstrated a strong association between EASM variability and the hydrological conditions as well as convective activity in the IPWP (e.g., Lau *et al.* 2000; Lu, 2001; Kawamura *et al.* 2001; Yin *et al.* 2014). The records of Chinese stalagmite $\delta^{18}O$, commonly used to reconstruct EASM variability, display distinct precession-related changes with intense precipitation during higher Northern Hemisphere summer insolation over the past 450 kyr (Fig. 5b; Cheng *et al.* 2016). The strong precession signal observed in Chinese speleothem records corresponding to insolation patterns is consistent with climate model simulations (e.g., Battisti *et al.* 2014; Rachmayani *et al.* 2016). The Site U1486 $\delta^{18}O_{sw\text{-}ivc}$ variations generally show a pronounced anti-phased relationship with Chinese stalagmite $\delta^{18}O$ on precessional timescales (Fig. 5b, f). This observation is further corroborated by the coherence analysis (Fig. 5h) and by most of the precipitation records within the IPWP region (Fig. 4). When $\delta^{18}O_{sw\text{-}ivc}$ values increase (lower precipitation) in the IPWP, the $\delta^{18}O$ values in Chinese speleothems decrease (higher precipitation). Conversely, periods of high precipitation in the IPWP correspond to a weakening of the EASM. Additionally, the simulated $\delta^{18}O_{sw\text{-}ivc}$ of the IPWP and measured $\delta^{18}O$ values in Chinese speleothems are anti-correlated on precessional timescales

https://doi.org/10.1017/S0016756824000177 Published online by Cambridge University Press

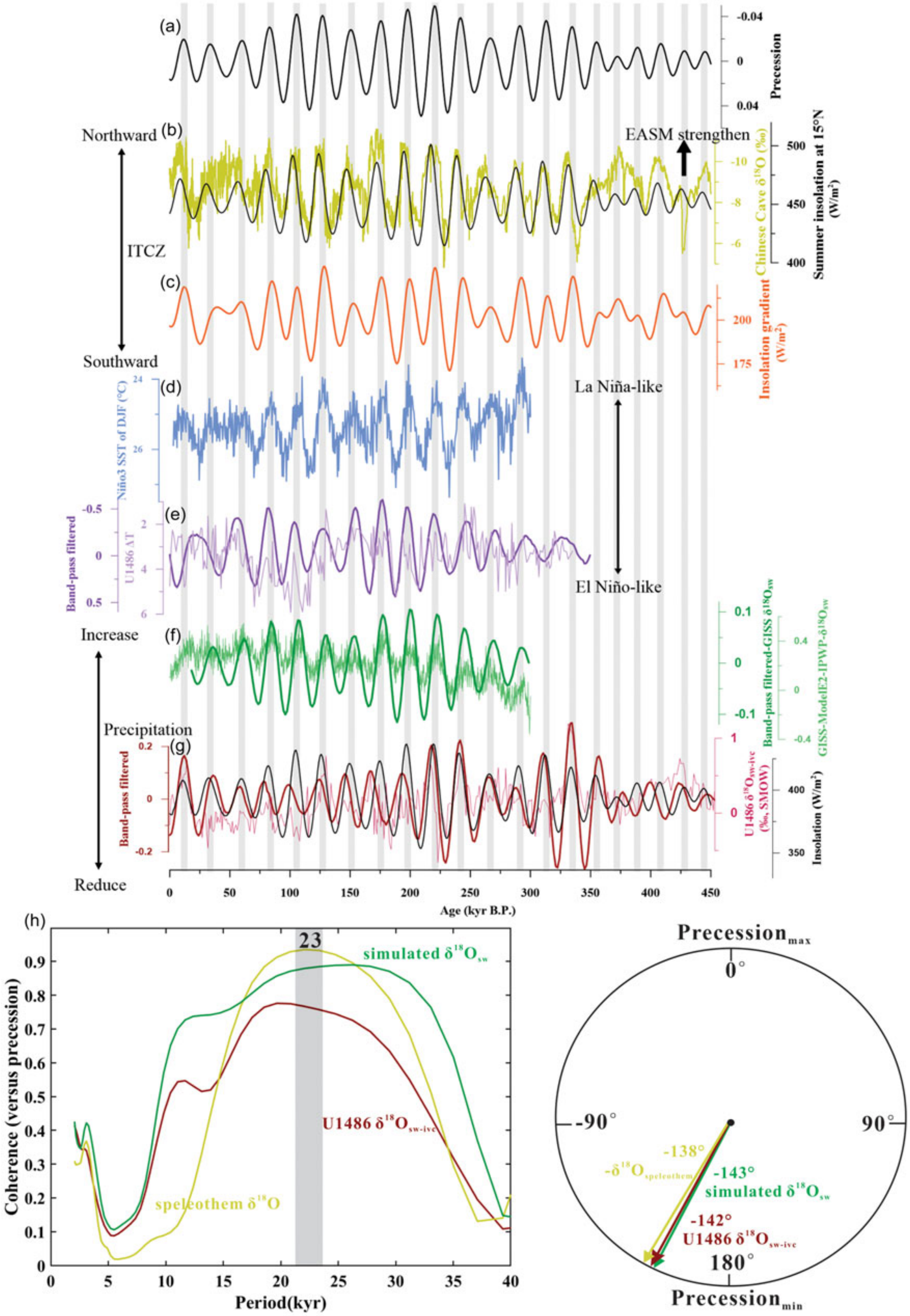

Figure 5. (Colour online) Comparing the precipitation records in the IPWP and East Asia with the ENSO-like proxy and the migration of the ITCZ. (a) The variation in precession (Laskar *et al*. 2004). (b) The speleothem $\delta^{18}O$ records in China (Cheng *et al*. 2016), superimposed on the summer insolation at 15°N (Laskar *et al*. 2004). (c) The summer interhemispheric tropical insolation gradient, determined by the variation in June insolation between 23° N and 23° S (Laskar *et al*. 2004). (d) CESM-simulated Niño3 SST of DJF (Zhang *et al*. 2021). (e) Differences between SST and thermocline water temperature (ΔT) for Site U1486. (f) GISS_ModelE2-R simulated $\delta^{18}O_{sw\text{-}ivc}$ records of the IPWP (Jian *et al*. 2022). (g) The $\delta^{18}O_{sw\text{-}ivc}$ records of Site U1486 superimposed by the July–August insolation at the equator (black) (Laskar *et al*. 2004). The records are overlaid by the precession band-pass filtered output (bold, dark-colored lines). Band-pass filter with a central frequency of 0.043 kyr^{-1} and a bandwidth of 0.01 kyr^{-1}. Vertical grey bars indicate lower precession values (high Northern Hemisphere summer insolation). (h) Phase relationships among U1486 $\delta^{18}O_{sw\text{-}ivc}$, simulated IPWP $\delta^{18}O_{sw\text{-}ivc}$, speleothem $\delta^{18}O$ and the precession parameter, illustrated through coherences (left) and phase angles (right).

https://doi.org/10.1017/S0016756824000177 Published online by Cambridge University Press

(Fig. 5b, e; Jian *et al.* 2022), which is further confirmed by cross-spectral analysis (Fig. 5h).

The anti-phased relationship between $\delta^{18}O_{sw\text{-}ivc}$ of the IPWP and Chinese speleothem $\delta^{18}O$ is associated with the ocean heat content of the IPWP (Jian *et al.* 2022). During low precession phases (high Northern Hemisphere summer insolation), La Niña-like conditions prevail in the western tropical Pacific. This is indicated by both the CESM-simulated Niño3 SST of December–January–February (DJF) (Zhang *et al.* 2021), and the temperature gradient between sea surface and thermocline waters (ΔT). A deep thermocline at Site U1486 deduced from a small ΔT (unpublished data) implies enhanced ocean heat storage in the mixed layer (Fig. 5d, e). This higher ocean heat content likely amplifies the strength of the EASM, enhancing moisture transport from ocean to continent and resulting in a negative deviation in Chinese speleothem $\delta^{18}O$ values (Jian *et al.* 2022). The precipitation changes in the IPWP and EASM regions exhibit a strong coherence to local insolation changes. Therefore, their precipitation changes may be attributed to the redistribution of heat between the Northern and Southern Hemispheres triggered/amplified by precessional forcing, a conclusion which is consistent with model simulations (Braconnot *et al.* 2008; Battisti *et al.* 2014).

The IPWP, located within the belt of the modern ITCZ's seasonal migration (Fig. 1a), experiences precipitation primarily regulated by the seasonal latitudinal movement of the ITCZ (Trenberth *et al.* 2000; Schmidt & Spero, 2011; Schneider *et al.* 2014; Jo *et al.* 2014). During periods of elevated summer insolation in the Northern Hemisphere, the ITCZ migrates northward (e.g., McGee *et al.* 2014), lowering precipitation in IPWP (Schmidt & Spero, 2011; Jo *et al.* 2014). This low in IPWP precipitation is supported by the high values of $\delta^{18}O_{sw\text{-}ivc}$ records from the IPWP region during the lower precession periods, which correspond to the high summer insolation in the Northern Hemisphere (Fig. 4). Seasonal variations in the thermal contrast between the Northern and Southern Hemispheres prompted the migration of the ITCZ, shifting toward the warmer hemisphere (Schneider *et al.* 2014). During the boreal summer, increasing insolation warms the subtropical water, strengthening the meridional pressure gradient and enhancing the southerlies flowing across the equator into the ITCZ, leading the ITCZ to move northward (Chang & Philander, 1994; Geen *et al.* 2020). Therefore, the migration of the mean position of the ITCZ could be indicated by the disparity in summer insolation between hemispheres (Chiang & Friedman 2012; Lu *et al.* 2013; Schneider *et al.* 2014). We calculated the summer interhemispheric insolation gradient between 23° N and 23° S (Fig. 5c; Laskar *et al.* 2004). A higher summer interhemispheric gradient during the precessional minima points to the northward migration of the ITCZ and reduced precipitation in the IPWP (Fig. 5f, g). Conversely, a decreased meridional summer interhemispheric insolation gradient results in the southward shift of the ITCZ, causing increased precipitation in the IPWP (Fig. 5c, f, g). During periods of Northern Hemisphere warming, such as the Bølling–Allerød and the early Holocene epochs characterized by a strong EASM, the ITCZ shifted northward (Wang *et al.* 2001; Yancheva *et al.* 2007). Recent research further suggests that the location and migrations of the ITCZ, where the trade winds of the Northern and Southern Hemispheres converge, are closely associated with variations in regional monsoon patterns (Gadgil, 2018, and references therein). Hence, the strength of the EASM is closely linked to the migrations of the ITCZ (e.g., Ding *et al.* 1995; An, 2000; Yancheva *et al.* 2007). Chinese stalagmite $\delta^{18}O$ records revealed that the intensification of the EASM during the precessional minima, accompanied by the northward migration of the ITCZ, resulting in high precipitation in the EASM region (Fig. 5b, c; Cheng *et al.* 2016). These findings emphasize the significant impact of ITCZ variations on hydrological changes within the IPWP and EASM regions. Orbital precession played a pivotal role in determining the seasonal distribution of incoming insolation in both hemispheres. This drives the north-south migration of the ITCZ and causes the subtropical high-pressure anomalies in the Indian and Pacific Oceans (Merlis *et al.* 2013; Schneider *et al.* 2014), leading to anti-correlated changes in precipitation between the IPWP and EASM region.

The mechanisms described above, supported by other paleoclimatic and modeling studies spanning millennial to orbital timescales (e.g., Wang *et al.* 2006; Merlis *et al.* 2013; Dang *et al.* 2015; Huang *et al.* 2019), provide a robust explanation for the interhemispheric anti-phased precipitation pattern between the IPWP and EASM region. Nevertheless, precipitation records in the northern equatorial region of the IPWP (e.g., cores MD06-3047B and MD06-3067; Bolliet *et al.* Bolliet *et al.*, 2011; Jia *et al.* Jia *et al.*, 2018) exhibit nearly synchronous interhemispheric changes with the southern IPWP region (Fig. 4). The migration of the ITCZ alone might not adequately account for the synchronous interhemispheric precipitation changes observed. Today, the ITCZ shifts between 9°N in boreal summer and 2°N in boreal winter across the modern Pacific Ocean (Schneider *et al.* 2014). We speculate that during periods of high precession when the ITCZ migrates southward, the ITCZ might still remain in the Northern Hemisphere, resulting in heightened precipitation over both the northern and southern IPWP regions. Besides, we propose that the synchronized interhemispheric precipitation changes in the northern and southern WPWP could be linked to the expansion and contraction of the ITCZ on the precession band (see below).

4.c.2. Variations in ITCZ expansion and contraction

Numerous studies have revealed the in-phase changes in precipitation between hemispheres over (sub-)millennial time-scales, which can be effectively explained by the expansion and contraction of the ITCZ, specifically its width (e.g., Collins *et al.* 2010; Konecky *et al.* 2013; Yan *et al.* 2015; Denniston *et al.* 2016; Scroxton *et al.* 2017; Yang *et al.* 2023). Yang *et al.* (2023) discovered that both the southern and northern margins of the ITCZ experienced simultaneously arid tropical Indian Ocean hydrological conditions during the early stage of the deglacial Heinrich Stadial 1 period, indicating a contracted tropical precipitation belt during that time. The precession bandpass filtered $\delta^{18}O_{sw\text{-}ivc}$ records of core MD06-3047B (located near the northern margin of the ITCZ), and Site U1483 and core MD05-2925 (located in the southern margin of the ITCZ) show reduced precipitation during most lower precession periods (Fig. 6b–d; Jia *et al.* Jia *et al.*, 2018; Zhang *et al.* 2022; Lo *et al.* 2022), possibly indicating the contraction of the ITCZ in the IPWP region and vice versa. While the precipitation records in the northern and southern marginal ITCZ are not consistently in-phase during certain periods (e.g., 390–360 ka BP), this discrepancy may be attributed to regional influencing factors or stratigraphical issues. However, collectively, these records consistently demonstrate high coherence with precession variability, suggesting that the ITCZ contracts during lower precession periods and expands during higher precession periods. We hypothesize that the synchronization of precipitation in both northern and southern regions of the IPWP on the precession band may also be attributed to the expansion and contraction of the ITCZ. Coincident with the ascending branch of

https://doi.org/10.1017/S0016756824000177 Published online by Cambridge University Press

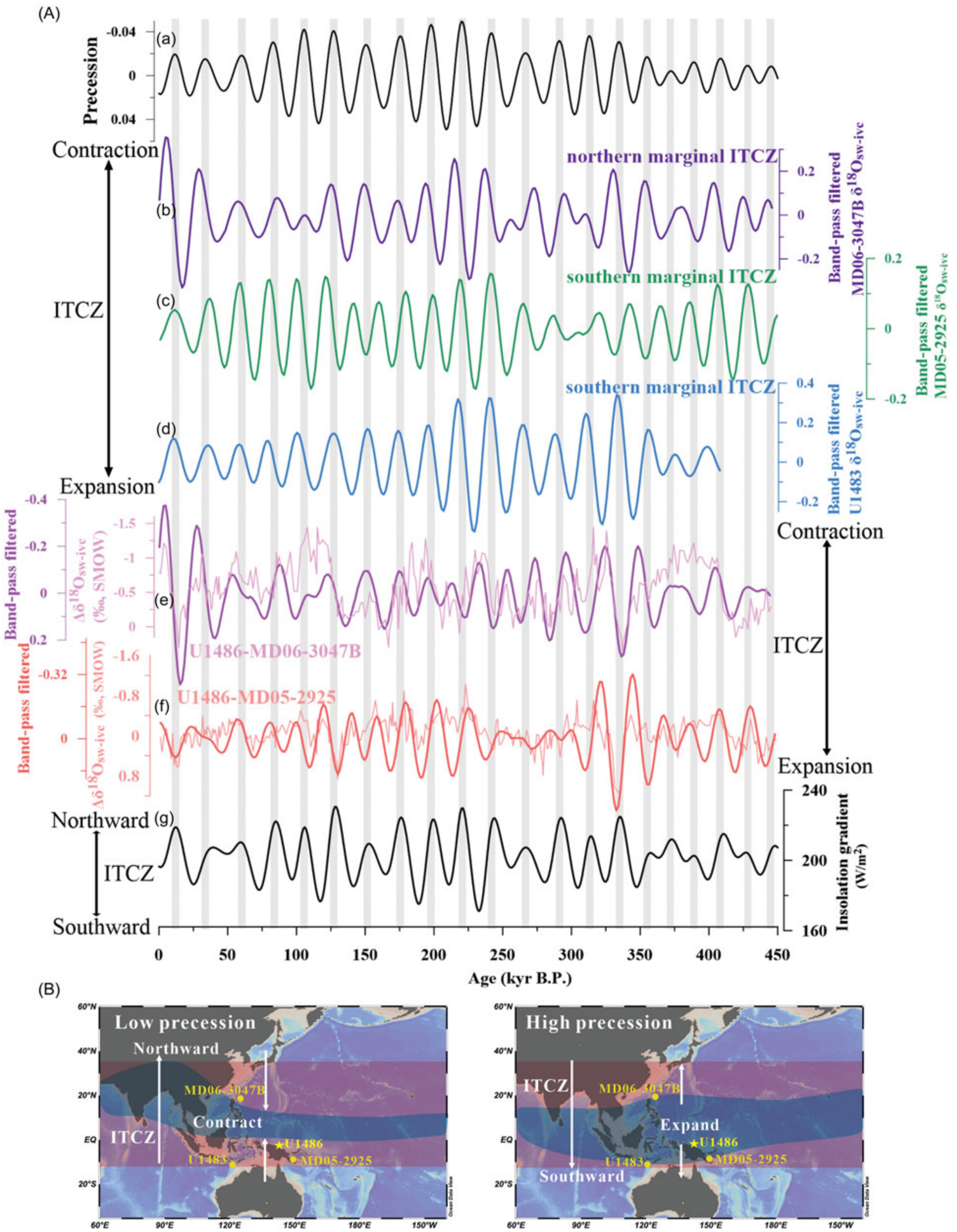

Figure 6. (Colour online) Effects of the ITCZ migration and width on the precipitation variations in the IPWP on the precession band. A. The records of ITCZ migration and width variation: (a) The variation in precession (Laskar *et al*. 2004). (b, c, d) Precession bandpass filtering curves of $\delta^{18}O_{sw\text{-}ivc}$ records in northern marginal ITCZ (core MD06-3047B; Jia *et al*. Jia *et al*., 2018) and southern marginal ITCZ (core MD05-2925 and Site U1483; Lo *et al*. 2022; Zhang *et al*. 2022). (e) Gradients of $\delta^{18}O_{sw-ivc}$ between Site U1486 and core MD06-3047B (Jia *et al*. Jia *et al*., 2018). (f) Gradients of $\delta^{18}O_{sw-ivc}$ between Site U1486 and core MD05-2925 (Lo *et al*. 2022). (g) The summer interhemispheric tropical insolation gradient, determined by the variation in June insolation between 23° N and 23° S (Laskar *et al*. 2004). Vertical grey bars indicate lower precession values. B. Schematic diagrams showing ITCZ variability during low-precession (left) and high-precession (right) intervals. The pink shaded band indicates the position and size of the ITCZ, referring to the belt of the modern ITCZ's seasonal migration.

the Hadley circulation, the ITCZ is typically delineated as the convergence zone of the trade winds from the Northern and Southern Hemispheres, thus strongly impacted by regional tropical climate dynamics (Byrne & Schneider, 2016; Geen *et al.* 2020). Studies suggest that on (sub)-millennial timescales, the ITCZ width may be linked to variations in the Walker circulation (Konecky *et al.* 2013) and meridional atmospheric circulation (Denniston *et al.* 2016). Consequently, we propose that synchronous precipitation changes between the hemispheres on orbital timescales might be intricately tied to changes in regional atmospheric circulation, which could affect the expansion and contraction of the ITCZ.

Yuan *et al.* (2023) suggested that the larger (smaller) discrepancy in rainfall between the central and marginal regions of the ITCZ corresponds to a more contracted (expanded) ITCZ. In our study, we calculated the differences in $\delta^{18}O_{sw\text{-}ivc}$ ($\Delta\delta^{18}O_{sw\text{-}ivc}$) among Site U1486 (central ITCZ), core MD06-3047B (near the northern marginal ITCZ) and core MD05-2925 (southern marginal ITCZ) to explore the variations in ITCZ contraction/expansion on orbital timescales (Fig. 6e, f). It should be noted that although $\delta^{18}O_{sw\text{-}ivc}$ may be influenced by various factors, we hypothesize that it primarily reflects changes in the precipitation-evaporation balance at the core sites in the IPWP, as discussed in Section 4.a. However, we acknowledge the presence of a leading or lagging relationship between $\Delta\delta^{18}O_{sw\text{-}ivc}$ and the expansion and contraction of the ITCZ on precession bands over the past 450 kyr (Fig. 6a, e, f), which does not exclude the possibility of $\delta^{18}O_{sw\text{-}ivc}$ being influenced by other factors or differences in core age models. We use this approach of $\Delta\delta^{18}O_{sw\text{-}ivc}$ to solely qualitatively describe the changes in ITCZ contraction and expansion during low-precession and high-precession intervals. Overall, the $\Delta\delta^{18}O_{sw\text{-}ivc}$ records between central and marginal ITCZ regions both increase during lower precession periods, while smaller precipitation differences (reduced $\Delta\delta^{18}O_{sw\text{-}ivc}$) indicate an expanded ITCZ during higher precession periods (Fig. 6e, f).

Yan *et al.* (2015) proposed that the ITCZ's expansion and contraction correspond with symmetrical changes in insolation between hemispheres on sub-millennial timescales. Furthermore, recent modeling work by Singarayer *et al.* (2017) indicate that precessional changes in the ITCZ width may result from different responses of its northern and southern extremes to variations in the interhemispheric temperature gradient. Thus, we suggest that variations in interhemispheric insolation due to precession may influence the expansion and contraction of the ITCZ. These hemispheric insolation variations could affect the interactions between radiation and clouds and thus ITCZ width, as suggested by the climate models (Voigt & Shaw, 2015; Lau & Kim, 2015). The contracted and expanded positions of the ITCZ, as depicted in Figure 6B, were determined based on various precipitation records across different IPWP regions, providing a qualitative overview of the ITCZ positions. Some studies suggests that the ITCZ might be influenced by extratropical forcing, such as the North Hemisphere ice sheet and the Atlantic meridional overturning circulation (Kang *et al.* 2008). If so, variations in the low/high precession parameter under different climate conditions could lead to differing latitudinal shifts and sizes of the ITCZ. However, in our study we hypothesize that position and size of the ITCZ remain constant under all low (high) precession periods. Here, the position and size refer to the belt of the modern ITCZ's seasonal migration (Fig. 1a). In summary, we suggest that the precessional hydroclimatic synchronicity changes in the IPWP might be driven by both the latitudinal migration of the ITCZ and the variations in its width over the past 450 kyr. The ITCZ migrated northward (southward) and contracted (expanded) during the periods of low (high) precession, as indicated by enriched (depleted) precipitation in the EASM region and in-phase depleted (enriched) precipitation in the entire IPWP region (Fig. 6B).

5. Conclusions

We utilized high-resolution $\delta^{18}O_{sw\text{-}ivc}$ records approximating SSS from Site U1486, retrieved from the Sepik River mouth in Papua New Guinea, to reconstruct precipitation changes within the IPWP over the past 450 kyr. The $\delta^{18}O_{sw\text{-}ivc}$ records display a dominant 23 kyr periodicity without a distinct glacial-interglacial trend. Our analysis focused on examining the spatial pattern of precipitation variations across the IPWP over orbital timescales, revealing a synchronous precipitation pattern on precession band. We assert that changes in ITCZ played a dominant role in determining the reconstructed precipitation patterns in the IPWP region on precession band. The anti-phased precipitation changes between the IPWP and the EASM region unveiled variations in the ITCZ migration, which was determined by the seasonal distribution of incoming insolation in both hemispheres on precession band. The synchronous precipitation changes between the two hemispheres within the IPWP emphasized the significant impact of the ITCZ's expansion and contraction on precipitation variability within the IPWP over precession timescales. Our findings suggest that during low precession periods, the ITCZ migrated northward and contracted, leading to increased precipitation in the EASM region and synchronous reduction of precipitation within the various locations across the IPWP.

Supplementary material. To view supplementary material for this article, please visit https://doi.org/10.1017/S0016756824000177

Acknowledgments. We thank all members of IODP Expedition 363 for their efforts in gathering the fundamental information and samples essential for this study. This study was financially supported by Laoshan Laboratory (No. LSKJ202204201), the Strategic Priority Research Program of the Chinese Academy of Sciences (Grant No. XDB42000000), and the National Natural Science Foundation of China (Grant Nos. 42076051, 42076050 and 41876041). We thank David McGee and Jiangnan Shi for providing useful feedback that improved the manuscript.

References

An ZS (2000) The history and variability of the East Asian paleomonsoon climate. *Quaternary Science Reviews* **19**, 171–87. doi: 10.1016/S0277-3791(99)00060-8

Barker S, Greaves M and Elderfield H (2003) A study of cleaning procedures used for foraminiferal Mg/Ca paleothermometry. *Geochemistry, Geophysics, Geosystems* **4**, 1–20. doi: 10.1029/2003gc000559

Battisti DS, Ding Q and Roe GH (2014) Coherent pan-Asian climatic and isotopic response to orbital forcing of tropical insolation. *Journal of Geophysical Research: Atmospheres* **119**, 11–997. doi: 10.1002/2014jd021960

Bemis BE, Spero HJ, Bijma J and Lea DW (1998) Reevaluation of the oxygen isotopic composition of planktonic foraminifera: experimental results and revised paleotemperature equations. *Paleoceanography* **13**, 150–60.

Berger A and Loutre MF (1994) Precession, eccentricity, obliquity, insolation and paleoclimates. In *Long-Term Climatic Variations. NATO ASI Series, vol 22* (eds JC Duplessy & MT Spyridakis) Berlin, Heidelberg: Springer. doi: 10.1007/978-3-642-79066-9_5

Berger AL (1978) Long-term variations of daily insolation and quaternary climate changes. *Journal of the Atmospheric Sciences* **35**, 2362–67.

https://doi.org/10.1017/S0016756824000177 Published online by Cambridge University Press

Bintanja R, van de Wal RS and Oerlemans J (2005) Modelled atmospheric temperatures and global sea levels over the past million years. *Nature* **437**, 125–28. doi: 10.1038/nature03975

Bolliet T, Holbourn A, Kuhnt W, Laj C, Kissel C, Beaufort L, Kienast M, Andersen N and Garbe-Schönberg D (2011) Mindanao Dome variability over the last 160 kyr: episodic glacial cooling of the West Pacific Warm Pool. *Paleoceanography* **26**, PA1208. doi: 10.1029/2010pa001966

Bosmans JHC, Drijfhout SS, Tuenter E, Hilgen FJ, Lourens LJ and Rohling EJ (2015) Precession and obliquity forcing of the freshwater budget over the Mediterranean. *Quaternary Science Reviews* **123**, 16–30. doi: 10.1016/j.quascirev.2015.06.008

Braconnot P, Marzin C, Gregoire L, Mosquet E and Marti O (2008) Monsoon response to changes in Earth's orbital parameters: comparisons between simulations of the Eemian and of the Holocene. *Climate of the Past* **4**, 281–94. doi: 10.5194/cp-4-281-2008

Byrne MP and Schneider T (2016) Narrowing of the ITCZ in a warming climate: physical mechanisms. *Geophysical Research Letters* **43**, 11–350. doi: 10.1002/2016gl070396

Cane MA (1998) A role for the tropical Pacific. *Science* **282**, 59–61.

Chang P and Philander SG (1994) A coupled ocean–atmosphere instability of relevance to the seasonal cycle. *Journal of the Atmospheric Sciences* **51**, 3627–48. doi: 10.1175/1520-0469(1994)051<3627: ACOIOR>2.0.CO;2

Cheng H, Edwards RL, Sinha A, Spotl C, Yi L, Chen S, Kelly M, Kathayat G, Wang X, Li X, Kong X, Wang Y, Ning Y and Zhang H (2016) The Asian monsoon over the past 640,000 years and ice age terminations. *Nature* **534**, 640–46. doi: 10.1038/nature18591

Chiang JCH and Friedman AR (2012) Extratropical cooling, interhemispheric thermal gradients, and tropical climate change. *Annual Review of Earth and Planetary Sciences* **40**, 383–412. doi: 10.1146/annurev-earth-042711-105545

Clement AC, Hall A and Broccoli A (2004) The importance of precessional signals in the tropical climate. *Climate Dynamics* **22**, 327–41. doi: 10.1007/s00382-003-0375-8

Clement AC, Seager R and Murtugudde R (2005) Why are there tropical warm pools? *Journal of Climate* **18**, 5294–311. doi: 10.1175/JCLI3582.1

Collins JA, Schefuß E, Heslop D, Mulitza S, Prange M, Zabel M, Tjallingii R, Dokken TM, Huang E, Mackensen A, Schulz M, Tian J, Zarriess M and Wefer G (2010) Interhemispheric symmetry of the tropical African rainbelt over the past 23,000 years. *Nature Geoscience* **4**, 42–5. doi: 10.1038/ngeo1039

Conroy JL, Thompson DM, Cobb KM, Noone D, Rea S and LeGrande AN (2017) Spatiotemporal variability in the delta (18)O-salinity relationship of seawater across the tropical Pacific Ocean. *Paleoceanography* **32**, 484–97. doi: 10.1002/2016PA003073

Dai A and Wigley TML (2000) Global patterns of ENSO-induced precipitation. *Geophysical Research Letters* **27**, 1283–86. doi: 10.1029/1999GL011140

Dang H, Jian Z, Kissel C and Bassinot F (2015) Precessional changes in the western equatorial Pacific Hydroclimate: a 240 kyr marine record from the Halmahera Sea, East Indonesia. *Geochemistry, Geophysics, Geosystems* **16**, 148–64. doi: 10.1002/2014gc005550

De Deckker P (2016) The Indo-Pacific Warm Pool: critical to world oceanography and world climate. *Geoscience Letters* **3**, 20. doi: 10.1186/s40562-016-0054-3

Dekens PS., Lea DW, Pak DK and Spero HJ (2002) core top calibration of Mg/Ca in tropical foraminifera: refining paleotemperature estimation. *Geochemistry, Geophysics, Geosystems* **3**, 1–29. doi: 10.1029/2001gc000200

Denniston RF, Ummenhofer CC, Wanamaker AD, Lachniet MS, Villarini G, Asmerom Y, Polyak VJ, Passaro KJ, Cugley J, Woods D and Humphreys WF (2016) Expansion and contraction of the Indo-Pacific tropical rain belt over the last three Millennia. *Scientific Reports* **6**, 34485. doi: 10.1038/srep34485

Ding ZL, Liu TS, Rutter NW, Yu ZW, Guo ZT and Zhu RX (1995) Ice-volume forcing of East-Asian winter monsoon variations in the past 800,000 years, *Quaternary Research* **44**, 149–59.

Fairbanks RG, Evans MN, Rubenstone JL, Mortlock RA, Broad K, Moore MD and Charles CD (1997) Evaluating climate indices and their geochemical proxies measured in corals. *Coral Reefs* **16**, S93–S100.

Gadgil S (2018) The monsoon system: land-sea breeze or the ITCZ? *Journal of Earth System Science* **127**, 1–29. doi: 10.1007/s12040-017-0916-x

Geen R, Bordoni S, Battisti DS and Hui K (2020) Monsoons, ITCZs, and the concept of the global monsoon. *Reviews of Geophysics* **58**, e2020RG000700. doi: 10.1029/2020rg000700

Gibbons FT, Oppo DW, Mohtadi M, Rosenthal Y, Cheng J, Liu Z and Linsley BK (2014) Deglacial δ^{18}O and hydrologic variability in the tropical Pacific and Indian Oceans. *Earth and Planetary Science Letters* **387**, 240–51. doi: 10.1016/j.epsl.2013.11.032

Hammer Ø, Harper D and Ryan P (2001) PAST-Paeontological Statistics, ver. 1.89. *Palaeontology Electron* **4**, 1–9.

Hoerling MP, Hurrell JW and Xu T (2001) Tropical origins for recent North Atlantic climate change. *Science* **292**, 90–2. doi: 10.1126/science.1058582

Holloway MD, Sime LC, Singarayer JS, Tindall JC and Valdes PJ (2016) Recon structing paleosalinity from δ^{18}O: coupled model simulations of the last glacial maximum, last interglacial and late Holocene. *Quaternary Science Reviews* **131**, 350–64. doi: 10.1016/j.quascirev.2015.07.007

Hollstein M, Mohtadi M, Kienast M, Rosenthal Y, Groeneveld J, Oppo DW, Southon JR and Lückge A (2020) The impact of astronomical forcing on surface and thermocline variability within the Western Pacific warm pool over the past 160 kyr. *Paleoceanography and Paleoclimatology* **35**, e2019PA003832. doi: 10.1029/2019pa003832

Hollstein M, Mohtadi M, Rosenthal Y, Moffa Sanchez P, Oppo D, Martínez Méndez G, Steinke S and Hebbeln D (2017) Stable oxygen isotopes and Mg/Ca in planktic foraminifera from modern surface sediments of the western Pacific warm pool: Implications for thermocline reconstructions. *Paleoceanography* **32**(11), 1174–1194. doi: 10.1002/2017pa003122

Huang J, Wan S, Li A and Li T (2019) Two-phase structure of tropical hydroclimate during Heinrich Stadial 1 and its global implications. *Quaternary Science Reviews* **222**, 105900. doi: 10.1016/j.quascirev.2019.105900

Hut G (1987) In: Consultants Group Meeting on Stable Isotopic Reference Samples for Geochemical and Hydrological Investigations. *International Atomic Energy Agency*, Vienna, p. 42.

Jalihal C, Bosmans JHC, Srinivasan J and Chakraborty A (2019) The response of tropical precipitation to earth's precession: the role of energy fluxes and vertical stability. *Climate of the Past* **15**, 449–62. doi: 10.5194/cp-15-449-2019

Jia Q, Li T, Xiong Z, Steinke S, Jiang F, Chang F and Qin B (2018) Hydrological variability in the western tropical Pacific over the past 700 kyr and its linkage to Northern Hemisphere climatic change. *Palaeogeography, Palaeoclimatology, Palaeoecology* **493**, 44–54. doi: 10.1016/j.palaeo.2017.12.039

Jian Z, Wang Y, Dang H, Mohtadi M, Rosenthal Y, Lea DW, Liu Z, Jin H, Ye L, Kuhnt W and Wang X (2022) Warm pool ocean heat content regulates ocean-continent moisture transport. *Nature* **612**, 92–9. doi: 10.1038/s41586-022-05302-y

Jo KN, Woo KS, Yi S, Yang DY, Lim HS, Wang Y, Cheng H and Edwards RL (2014) Mid-latitude interhemispheric hydrologic seesaw over the past 550,000 years. *Nature* **508**, 378–82. doi: 10.1038/nature13076

Kang SM, Held IM, Frierson DMW and Zhao M (2008) The response of the ITCZ to extratropical thermal forcing: idealized slab-Ocean experiments with a GCM. *Journal of Climate* **21**, 3521–32. doi: 10.1175/2007jcli2146.1

Kawamura R, Matsuura T and Iizuka S (2001) Role of equatorial asymmetric sea surface temperature anomalies in the Indian Ocean on the Asian summer monsoon and El Nino–southern oscillation coupling. *Journal of Geophysical Research* **106**, 4681–93. doi: 10.1029/2000JD900610

Kim ST, Yu JY and Lu MM (2012) The distinct behaviors of Pacific and Indian Ocean warm pool properties on seasonal and interannual time scales. *Journal of Geophysical Research: Atmospheres* **117**, D05128. doi: 10.1029/2011jd016557

Kissel C, Laj C, Kienast M, Bolliet T, Holbourn A, Hill P, Kuhnt W and Braconnot P (2010) Monsoon variability and deep oceanic circulation in the western equatorial Pacific over the last climatic cycle: insights from sedimentary magnetic properties and sortable silt. *Paleoceanography* **25**, PA3215. doi: 10.1029/2010pa001980

Konecky BL, Russell JM, Rodysill JR, Vuille M, Bijaksana S and Huang Y (2013) Intensification of southwestern Indonesian rainfall over the past millennium. *Geophysical Research Letters* **40**, 386–91. doi: 10.1029/2012gl054331

https://doi.org/10.1017/S0016756824000177 Published online by Cambridge University Press

Kutzbach JE, Liu X, Liu Z and Chen G (2008) Simulation of the evolutionary response of global summer monsoons to orbital forcing over the past 280,000 years. *Climate Dynamics* **30**, 567–79. doi: 10.1007/s00382-007-0308-z

Laskar J, Robutel P, Joutel F, Gastineau M, Correia ACM and Levrard B (2004) A long-term numerical solution for the insolation quantities of the Earth. *Astronomy & Astrophysics* **428**, 261–85.

Lau KM and Kim KM (2015) Robust Hadley circulation changes and increasing global dryness due to CO2 warming from CMIP5 model projections. *Proceedings of the National Academy of Sciences* **112**, 3630–35. doi: 10.1073/pnas.1418682112

Lau KM, Kim KM and Yang S (2000) Dynamical and boundary forcing characteristics of regional components of the Asian summer monsoon. *Journal of Climate* **13**, 2461–82. doi: 10.1175/1520-0442(2000)013<2461:DABFCO>2.0.CO;2

Lea DW, Pak DK and Spero HJ (2000) Climate impact of late quaternary equatorial pacific sea surface temperature variations. *Science* **289**, 1719–24. doi: 10.1126/science.289.5485.1719

Leech PJ, Lynch-Stieglitz J and Zhang R (2013) Western pacific thermocline structure and the pacific marine intertropical convergence zone during the last glacial maximum. *Earth and Planetary Science Letters* **363**, 133–43. doi: 10.1016/j. epsl.2012.12.026

LeGrande AN and Schmidt GA (2006) Global gridded data set of the oxygen isotopic composition in seawater. *Geophysical Research Letters* **33**, L12604. doi: 10.1029/2006GL026011

Leung JCH, Zhang B, Gan Q, Wang L, Qian W and Hu ZZ (2022) Differential expansion speeds of Indo-Pacific warm pool and deep convection favoring pool under greenhouse warming. *npj Climate and Atmospheric Science* **5**, 97. doi: 10.1038/s41612-022-00315-w

Lisiecki L and Raymo M (2005) A Pliocene-Pleistocene stack of 57 globally distributed benthic $\delta^{18}O$ records. *Paleoceanography* **20**, PA1003. doi: 10.1029/2004PA001071

Liu Y, Lo L, Shi Z, Wei KY, Chou CJ, Chen YC, Chuang CK, Wu CC, Mii HS, Peng Z, Amakawa H, Burr GS, Lee SY, DeLong KL, Elderfield H and Shen CC (2015) Obliquity pacing of the western Pacific Intertropical Convergence Zone over the past 282,000 years. *Nat Commun* **6**, 10018. doi: 10.1038/ncomms10018

Lo L, Shen CC, Zeeden C, Tsai YH, Yin Q, Yang CC, Chang TL, Su YC, Mii HS, Chuang CK and Chen YC (2022) Orbital control on the thermocline structure during the past 568 kyr in the Solomon Sea, southwest equatorial Pacific. *Quaternary Science Reviews* **295**, 107756. doi: 10.1016/j.quascirev.2022.107756

Locarnini RA, Mishonov AV, Antonov JI, Boyer TP, Garcia HE, Baranova OK, Zweng MM, Paver CR, Reagan JR, Johnson DR, Hamilton M and Seidov D (2013) World Ocean Atlas 2013. Volume 1, temperature. In *NOAA Atlas NESDIS, vol. 73* (eds S Levitus, A Mishonov & Technical), p. 40, Publication. doi: 10.7289/V55X26VD

Lu H, Yi S, Liu Z, Mason JA, Jiang D, Cheng J, Stevens T, Xu Z, Zhang E, Jin L, Zhang Z, Guo Z, Wang Y and Otto-Bliesner B (2013) Variation of East Asian monsoon precipitation during the past 21 k.y. and potential CO_2 forcing. *Geology* **41**, 1023–26. doi: 10.1130/G34488.1

Lu RY (2001) Interannual variability of the summer time North Pacific subtropical high and its relation to atmospheric convection over the Warm Pool. *Journal of the Meteorological Society of Japan Ser II* **79**, 771–83.

Lutgens FK and Tarbuck EJ (2001) *The atmosphere* (8th ed.). Upper Saddle River, NJ: Prentice Hall.

Mantsis DF, Clement AC, Broccoli AJ and Erb MP (2011) Climate feedbacks in response to changes in obliquity. *Journal of Climate*, **24**(11), 2830–2845. doi: 10.1175/2010JCLI3986.1

Mantsis DF, Lintner BR, Broccoli AJ, Erb MP, Clement AC and Park H (2014) The response of large-scale circulation to obliquity-induced changes in meridional heating gradients. *Journal of Climate*, **27**(14), 5504–5516. doi: 10.1175/JCLI-D-13-00526.1

McGee D, Donohoe A, Marshall J and Ferreira D (2014) Changes in ITCZ location and cross-equatorial heat transport at the Last Glacial Maximum, Heinrich Stadial 1, and the mid-Holocene. *Earth and Planetary Science Letters* **390**, 69–79. doi: 10.1016/j.epsl.2013.12.043

Merlis TM, Schneider T, Bordoni S and Eisenman I (2013) The tropical precipitation response to orbital precession. *Journal of Climate* **26**, 2010–21. doi: 10.1175/jcli-d-12-00186.1

Mohtadi M, Prange M, Oppo DW, De Pol-Holz R, Merkel U, Zhang X, Steinke S and Luckge A (2014) North Atlantic forcing of tropical Indian Ocean climate. *Nature* **509**, 76–80. doi: 10.1038/nature13196

Nürnberg D, Bijma J and Hemleben C (1996) Assessing the reliability of magnesium in foraminiferal calcite as a proxy for water mass temperatures. *Geochimica et Cosmochimica Acta* **60**, 803–14. doi: 10.1016/0016-7037(95)00446-7

Pierrehumbert RT (2000) Climate change and the Tropical Pacific: the sleeping Dragon Wakes. *Proceedings of the National Academy of Sciences* **97**, 1355–58. doi: 10.1073/pnas.97.4.1355

Qian F, Chang F, Li T, Li A, Sun H and Zhang J (2023) Thermocline variability in the subtropical northwestern Pacific since the last deglaciation. *Palaeogeography, Palaeoclimatology, Palaeoecology* **612**, 111379. doi: 10.1016/j.palaeo.2022.111379

Rachmayani R, Prange M and Schulz M (2016) Intra-interglacial climate variability: model simulations of Marine Isotope Stages 1, 5, 11, 13, and 15. *Climate of the Past* **12**, 677–95. doi: 10.5194/cp-12-677-2016

Raddatz J, Nürnberg D, Tiedemann R and Rippert N (2017) Southeastern marginal West Pacific Warm Pool sea-surface and thermocline dynamics during the Pleistocene (2.5–0.5 Ma). *Palaeogeography, Palaeoclimatology, Palaeoecology* **471**, 144–56. doi: 10.1016/j.palaeo.2017.01.024

Regenberg M, Nürnberg D, Steph S, Groeneveld J, Garbe-Schönberg D, Tiedemann R and Dullo WC (2006) Assessing the effect of dissolution on planktonic foraminiferal Mg/Ca ratios: evidence from Caribbean core tops. *Geochemistry, Geophysics, Geosystems* **7**, Q07P15. doi: 10.1029/2005gc001019

Regenberg M, Regenberg A, Garbe-Schönberg D and Lea DW (2014) Global dissolution effects on planktonic foraminiferal Mg/Ca ratios controlled by the calcite-saturation state of bottom waters. *Paleoceanography* **29**, 127–42. doi: 10.1002/2013pa002492

Rippert N, Nürnberg D, Raddatz J, Maier E, Hathorne E, Bijma J and Tiedemann R (2016) Constraining foraminiferal calcification depths in the western Pacific warm pool. *Marine Micropaleontology* **128**, 14–27. doi: 10.1016/j.marmicro.2016.08.004

Rosenthal Y, Holbourn AE, Kulhanek DK and the Expedition 363 Scientists (2018) Western Pacific Warm Pool. Proceedings of the International Ocean Discovery Program, 363: College Station, TX (International Ocean Discovery Program). doi: 10.14379/iodp.proc.363.107.2018.

Rosenthal Y, Oppo DW and Linsley BK (2003) The amplitude and phasing of climate change during the last deglaciation in the Sulu Sea, western equatorial Pacific. *Geophysical Research Letters* **30**, 1428. doi: 10.1029/2002gl016612

Ruddiman WF (2008) *Earth's Climate: Past and Future*. 2nd ed. W. H. New York: Freeman and Company, 388 p.

Russell JM, Vogel H, Konecky BL, Bijaksana S, Huang Y, Melles M, Wattrus N, Costa K and King JW (2014) Glacial forcing of central Indonesian hydroclimate since 60,000 y B.P. *Proceedings of the National Academy of Sciences (U.S.A.)* **111**, 5100–05. doi: 10.1073/pnas.1402373111

Schmidt MW and Spero HJ (2011) Meridional shifts in the marine ITCZ and the tropical hydrologic cycle over the last three glacial cycles. *Paleoceanography* **26**, PA1206. doi: 10.1029/2010pa001976

Schneider T, Bischoff T and Haug GH (2014) Migrations and dynamics of the intertropical convergence zone. *Nature* **513**, 45–53. doi: 10.1038/nature13636

Scroxton N, Burns SJ, McGee D, Hardt B, Godfrey LR, Ranivoharimanana L and Faina P (2017) Hemispherically in-phase precipitation variability over the last 1700 years in a Madagascar speleothem record. *Quaternary Science Reviews* **164**, 25–36. doi: 10.1016/j.quascirev.2017.03.017

Singarayer JS, Valdes PJ and Roberts WHG (2017) Ocean dominated expansion and contraction of the late Quaternary tropical rainbelt. *Scientific Reports* **7**, 9382. doi: 10.1038/s41598-017-09816-8

Spratt RM and Lisiecki LE (2016) A late pleistocene sea level stack. *Climate of the Past* **12**(4), 1079–1092. doi: 10.5194/cp-12-1079-2016

https://doi.org/10.1017/S0016756824000177 Published online by Cambridge University Press

Stott L, Cannariato K, Thunell R, Haug GH, Koutavas A and Lund S (2004) Decline of surface temperature and salinity in the western tropical Pacific Ocean in the Holocene epoch. *Nature* **431**, 56–9. doi: 10.1038/nature02903

Tachikawa K, Cartapanis O, Vidal L, Beaufort L, Barlyaeva T and Bard E (2011) The precession phase of hydrological variability in the Western Pacific Warm Pool during the past 400 ka. *Quaternary Science Reviews* **30**, 3716–27. doi: 10.1016/j.quascirev.2011.09.016

Tachikawa K, Timmermann A, Vidal L, Sonzogni C and Timm OE (2014) CO_2 radiative forcing and Intertropical Convergence Zone influences on western Pacific warm pool climate over the past 400ka. *Quaternary Science Reviews* **86**, 24–34. doi: 10.1016/j.quascirev.2013.12.018

Trenberth KE, Stepaniak DP and Caron JM (2000) The global monsoon as seen through the divergent atmospheric circulation. *Journal of Climate* **13**, 3969–93. doi: 10.1175/1520-0442(2000)013<3969: Tgmast>2.0.Co;2

Voigt A and Shaw T (2015) Circulation response to warming shaped by radiative changes of clouds and water vapour. *Nature Geoscience* **8**, 102–6. doi: 10.1038/ngeo2345

Wang B, Wu R and Li T (2003) Atmosphere-warm ocean interaction and its impacts on Asian-Australian monsoon variation. *Journal of Climate* **16**, 1195–211. doi: 10.1175/1520-0442(2003)16<1195:AOIAII>2.0.CO;2

Wang X, Auler AS, Edwards RL, Cheng H, Ito E and Solheid M (2006) Interhemispheric anti-phasing of rainfall during the last glacial period. *Quaternary Science Reviews* **25**, 3391–403. doi: 10.1016/j.quascirev.2006.02.009

Wang Y, Cheng H, Edwards RL, Kong X, Shao X, Chen S, Wu J, Jiang X, Wang X and An Z (2008) Millennial- and orbital-scale changes in the East Asian monsoon over the past 224,000 years. *Nature* **451**, 1090–93. doi: 10.1038/nature06692

Wang YJ, Cheng H, Edwards RL, An ZS, Wu JY, Shen CC and Dorale JA (2001) A high-resolution absolute-dated late Pleistocene monsoon record from Hulu Cave, China. *Science* **294**, 2345–48. doi: 10.1126/science.1064618

Webster PJ, Magana VO, Palmer TN, Shukla J, Tomas RA, Yanai M and Yasunari T (1998) Monsoon: processes, predictability, and prospects for prediction. *Journal of Geophysical Research* **103**, 14,451–510.

Xiong Z, Zhai B, Algeo TJ, Lu Z, Li T, Meyer H, Jiang F, Zhang P, Qin B, Gong X, Wang Zand Jia Q (2022) Intensified aridity over the Indo-Pacific Warm Pool controlled by ice-sheet expansion during the Last Glacial Maximum. *Global and Planetary Change* **217**, 103952. doi: 10.1016/j.gloplacha.2022.103952

Yan H, Wei W, Soon W, An Z, Zhou W, Liu Z, Wang Y and Carter RM (2015) Dynamics of the intertropical convergence zone over the western Pacific during the Little Ice Age. *Nature Geoscience* **8**, 315–20. doi: 10.1038/ngeo23795

Yan XH, Ho CR, Zheng Q and Klemas V (1992) Temperature and size variabilities of the Western pacific warm pool. *Science* **258**, 1643–45.

Yancheva G, Nowaczyk NR, Mingram J, Dulski P, Schettler G, Negendank JF, Liu J, Sigman DM, Peterson LC and Haug GH (2007) Influence of the intertropical convergence zone on the East Asian monsoon. *Nature* **445**, 74–7. doi: 10.1038/nature05431

Yang L, Zhou W, Yan H, Ma X, Cheng P, Hu B, Shen X, Zhao H, Hou Y, Lu X and Liu C (2024). Step-wise shifted rainbelt throughout the early last deglaciation. *Global and Planetary Change* **232**, 104325. doi: 10.1016/j.gloplacha.2023.104325

Yang Y, Zhang L, Yi L, Zhong F, Lu Z, Wan S, Du Y and Xiang R (2023) A contracting intertropical convergence zone during the Early Heinrich Stadial 1. *Nature Communications* **14**, 4695. doi: 10.1038/s41467-023-40377-9

Yin QZ, Singh UK, Berger A, Guo ZT and Crucifix M (2014) Relative impact of insolation and the Indo-Pacific warm pool surface temperature on the East Asia summer monsoon during the MIS-13 interglacial. *Climate of the Past* **10**, 1645–57. doi: 10.5194/cp-10-1645-2014

Yin QZ, Wu ZP, Berger A, Goosse H and Hodell D (2021) Insolation triggered abrupt weakening of Atlantic circulation at the end of interglacials. *Science* **373**, 1035–40. doi: 10.1126/science.abg1737

Yu Z, Tang X, Colin C, Wilson DJ, Zhou X, Song L, Chang F, Zhang S, Bassinot F and Wan S (2023) Millennial-scale precipitation variability in the Indo-Pacific region over the Last 40 Kyr. *Geophysical Research Letters* **50**, e2022GL101646. doi: 10.1029/2022gl101646

Yuan S, Chiang H, Liu G, Bijaksana S, He S, Jiang X, Imran A, Wicaksono S and Wang X (2023) The strength, position, and width changes of the intertropical convergence zone since the Last Glacial Maximum. *Proceedings of the National Academy of Sciences* **120**, e2217064120. doi: 10.1073/pnas.2217064120

Zhang P, Xu J, Holbourn A, Kuhnt W, Beil S, Li T, Xiong Z, Dang H, Yan H, Pei R, Ran Y and Wu H (2020) Indo-Pacific hydroclimate in response to changes of the intertropical convergence zone: discrepancy on precession and obliquity bands over the last 410 kyr. *Journal of Geophysical Research: Atmospheres* **125**, e2019JD032125. doi: 10.1029/2019jd032125

Zhang P, Xu J, Holbourn A, Kuhnt W, Xiong Z and Li T (2022) Obliquity induced latitudinal migration of the intertropical convergence zone during the past ~410 kyr. *Geophysical Research Letters* **49**, e2022GL100039. doi: 10.1029/2022gl100039

Zhang S, Li T, Chang F, Yu Z and Wang H (2015) The relationship between the Tropical Pacific precipitation and the ITCZ variation since MIS 6. *Quaternary Sciences* **35**, 390–400. doi: 10.11928/j.issn.1001-7410.2015.02.14

Zhang S, Yu Z, Gong X, Wang Y, Chang F, Lohmman G, Qi Y and Li T (2021) Precession cycles of the El Niño/Southern oscillation-like system controlled by Pacific upper-ocean stratification. *Communications Earth & Environment* **2**, 239. doi: 10.1038/s43247-021-00305-5

https://doi.org/10.1017/S0016756824000177 Published online by Cambridge University Press